

UCSF

UC San Francisco Previously Published Works

Title

Heteroaryl Phosphonates as Noncovalent Inhibitors of Both Serine- and Metalloproteinases

Permalink

<https://escholarship.org/uc/item/9qz7885v>

Journal

Journal of Medicinal Chemistry, 62(18)

ISSN

0022-2623

Authors

Pemberton, Orville A
Jaishankar, Priyadarshini
Akhtar, Afroza
[et al.](#)

Publication Date

2019-09-26

DOI

10.1021/acs.jmedchem.9b00728

Peer reviewed



Published in final edited form as:

J Med Chem. 2019 September 26; 62(18): 8480–8496. doi:10.1021/acs.jmedchem.9b00728.

Heteroaryl phosphonates as non-covalent inhibitors of both serine- and metallo-carbapenemases

Orville A. Pemberton¹, Priyadarshini Jaishankar², Afroza Akhtar¹, Jessie L. Adams³, Lindsey N. Shaw³, Adam R. Renslo^{2,*}, Yu Chen^{1,*}

¹Department of Molecular Medicine, University of South Florida Morsani College of Medicine, 12901 Bruce B. Downs Blvd, MDC 3522, Tampa, Florida 33612, United States

²Department of Pharmaceutical Chemistry and Small Molecule Discovery Center, University of California San Francisco, 600 16th Street, Genentech Hall N574, San Francisco, California 94158, United States

³Department of Cell Biology, Microbiology & Molecular Biology, University of South Florida, 4202 E. Fowler Ave., Tampa, Florida 33620, United States

Abstract

Gram-negative pathogens expressing serine β -lactamases (SBLs) and metallo- β -lactamases (MBLs), especially those with carbapenemase activity, threaten the clinical utility of almost all β -lactam antibiotics. Here we describe the discovery of a heteroaryl phosphonate scaffold that exhibits non-covalent cross-class inhibition of representative carbapenemases, specifically the SBL KPC-2 and the MBLs NDM-1 and VIM-2. The most potent lead, compound **16**, exhibited low nM to low μ M inhibition of KPC-2, NDM-1, and VIM-2. Compound **16** potentiated imipenem efficacy against resistant clinical and laboratory bacterial strains expressing carbapenemases, while showing some cytotoxicity toward human HEK293T cells only at concentrations above 100

*Corresponding Author Information: Phone: (415) 514-9698. Fax: (415) 514-4507. adam.renslo@ucsf.edu, Phone: (813) 974-7809. Fax: (813) 974-7357. ychen1@health.usf.edu.

Author contributions

O.A.P. performed the molecular docking, biochemical, and X-ray crystallographic experiments. P.J. synthesized compounds. A.A. determined NDM-1 and VIM-2 crystal structures at pH 7. J. L. A. and L. N. S. performed the cell-based assays. O.A.P., A.R.R. and Y.C. designed the experiments and wrote the manuscript. All authors discussed the results and commented on the manuscript.

Supporting Information

The Supporting Information is available free of charge on the ACS Publications website.

Additional figures of IC₅₀ curves, complex structures of phosphonate compounds with KPC-2, NDM-1, and VIM-2, cytotoxicity testing, ¹H NMR spectra of synthetic analogs, table of crystallographic data collection and refinement statistics.

Molecular formula strings.

PDB ID

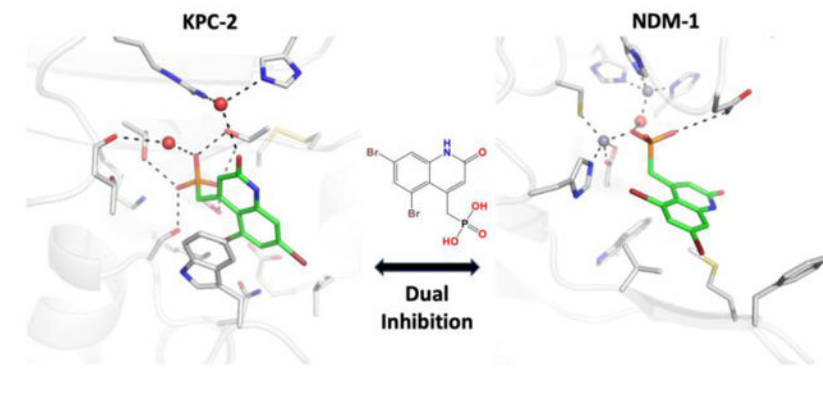
Coordinates and structure factors have been deposited in the Protein Data Bank (PDB) under accession codes 6D15 (KPC-2 with compound **1**), 6D16 (KPC-2 with compound **2**), 6D17 (KPC-2 with compound **3**), 6D18 (KPC-2 with compound **6**), 6D19 (KPC-2 with compound **9**), 6D1A (NDM-1 with compound **1**), 6D1B (NDM-1 with compound **2**), 6D1C (NDM-1 with compound **3**), 6D1D (NDM-1 with compound **6**), 6D1E (NDM-1 with compound **7**), 6D1F (NDM-1 with compound **8**), 6D1G (NDM-1 with compound **9**), 6D1H (NDM-1 with compound **11**), 6D1I (NDM-1 with compound **12**), 6D1J (NDM-1 with compound **13**), 6D1K (NDM-1 with compound **14**), 6DD0 (VIM-2 with compound **8**), 6DD1 (VIM-2 with compound **14**), 6O3R (NDM-1 D199N with compound **7**), 6NY7 (NDM-1 D199N with compound **16**) and 6O5T (VIM-2 with compound **16**). Crystallographic data collection and refinement statistics are summarized in Supporting Information Table 1. Authors will release the atomic coordinates and experimental data upon article publication.

Competing financial interests

O.A.P., P.J., A.R.R., and Y.C. are listed as inventors on a patent application describing compounds studied herein.

$\mu\text{g/mL}$. Complex structures with KPC-2, NDM-1, and VIM-2 demonstrate how these inhibitors achieve high binding affinity to both enzyme classes. These findings provide a structurally and mechanistically new scaffold for drug discovery targeting multidrug resistant Gram-negative pathogens, and more generally highlight the active site features of carbapenemases that can be leveraged for lead discovery.

Graphical Abstract



Introduction

The penicillins were among the first effective antibiotics, and current generation β -lactams such as the cephalosporins and carbapenems remain crucial agents in the treatment of serious, life-threatening bacterial infections¹. Resistance to β -lactam antibiotics most commonly involves the production of β -lactamase enzymes that hydrolyze the β -lactam ring². There are four classes of β -lactamase (A, B, C, and D), which differ from one another based on their amino acid sequence and mechanism of action. Classes A, C, and D are serine β -lactamases (SBLs), whereas class B are metallo- β -lactamases (MBLs) that use either one or two zinc ions to promote the hydrolysis reaction^{3, 4}.

Carbapenems (e.g., imipenem, meropenem, doripenem, and ertapenem) are often considered to be “last-resort” antibiotics on account of their effectiveness in treating serious, multidrug resistant infections⁵⁻⁷. Unfortunately, the recent emergence of carbapenem-resistant *Enterobacteriaceae* (CRE) and multidrug resistant *Pseudomonas aeruginosa* threatens the utility of all currently available β -lactam antibiotics. CRE and *P. aeruginosa* infections are associated with high rates of morbidity and mortality worldwide due to limited treatment options⁸⁻¹⁰. Carbapenem resistance in CRE and *P. aeruginosa* can be mediated by several factors, especially by the production of carbapenemases¹¹⁻¹³. Carbapenemase activity is exhibited by some class A and D SBLs and by all class B MBLs^{14, 15}. Most serine carbapenemases are versatile enzymes that can hydrolyze nearly all β -lactam substrates^{7, 14}. While MBLs also have a broad substrate spectrum, they are unable to catalyze the hydrolysis of monobactams^{4, 16, 17}. Among carbapenemases, of greatest concern currently are the class A SBL KPC-2 and the MBLs NDM-1 and VIM-2, all of which are commonly isolated from CRE, *P. aeruginosa*, and other Gram-negative pathogens¹⁶.

A number of β -lactamase inhibitors have been developed to address the growing problem of β -lactam antibiotic resistance, although currently marketed agents target only SBLs and not MBLs^{16, 18}. Classical β -lactamase inhibitors like clavulanic acid are active against many class A SBLs but possess limited activity against class C and D SBLs, and no activity against most serine or metallo-carbapenemases^{16, 19}. Newer, non- β -lactam derived compounds like avibactam²⁰ cover an expanded spectrum of class A, C, and D SBLs, including KPC-2, but are inactive against MBLs^{21, 22}. Notwithstanding some recent progress with boronic acid-based inhibitors^{23, 24}, finding cross-class inhibitor leads remains a significant and challenging problem²⁵.

In this study, we used structure-based design, synthetic chemistry, and X-ray crystallography to identify and explore common features of non-covalent small molecule binding by SBLs and MBLs. We identified a heteroaryl phosphonate scaffold with low μM to low nM affinities against KPC-2, NDM-1, and VIM-2, that also exhibits promising cell-based activity and good lead-like properties. Complex crystal structures of several analogs have revealed underappreciated structural features that likely underlie the broad substrate spectrum of carbapenemases. Taken together, these data offer a new chemotype and actionable information to guide development of new agents to counter carbapenemase-mediated resistance in pathogenic Gram-negative bacteria.

Results

A novel inhibitor chemotype for the KPC-2 serine carbapenemase

To develop novel inhibitor chemotypes, we sought to identify fragment- or lead-sized compounds that bound with high ligand efficiency (L.E.) (defined as binding enthalpy per non-H atom)²⁶ to the SBL KPC-2. The decision to start with KPC-2 was based on the expectation that ligand affinity for KPC-2 would derive from non-covalent interactions with active-site residues, while screening against MBLs could be dominated by chelation-driven interactions²⁷. We thus performed molecular docking of KPC-2 using the ZINC database²⁸ and identified several hits, including the coumarin-4-methylphosphonate **1** that is the focus of the current study (Table 1).

Using a biochemical assay with the nitrocefin substrate, we observed **1** to be a moderately potent and ligand-efficient inhibitor of KPC-2 ($K_i = 32.9 \mu\text{M}$; L.E. = $0.34 \text{ kcal mol}^{-1} \text{ heavy atom}^{-1}$). To probe SAR around this hit, we identified five related commercial analogs (**2-6**) that differed in substitution at positions C5-C7 of the coumarin ring. The potencies and ligand efficiencies of analogs **2-5** revealed that substitution at C7, as well as a lack of substitution at C6, were important for activity. Thus, regioisomers **4** and **5** bearing methyl groups at C7 or C6, respectively, exhibited K_i (and L.E.) values of $23.3 \mu\text{M}$ ($0.38 \text{ kcal mol}^{-1} \text{ HA}^{-1}$) and $154.4 \mu\text{M}$ ($0.31 \text{ kcal mol}^{-1} \text{ HA}^{-1}$) against KPC-2. Analogs **2** and **6**, both unsubstituted at C6, were the most potent and ligand efficient of the commercial analogs, with K_i values in the low- μM regime and L.E. values of 0.39 and 0.45, respectively.

Having established an apparent preference for substitution at both C5 and C7 (as in compound **6**), we evaluated additional, similarly substituted synthetic analogs. First, the steric and electronic character of the C5 substituent was modified systematically in analogs

sharing a C7-Me group (compounds **7**, **9**, **10**). Increasing the size of the C5 substituent from -F to -CH₃ to -Br improved potency and ligand efficiency, with the C5-Br analog **9** providing a new benchmark in potency and ligand efficiency ($K_i = 0.246 \mu\text{M}$; L.E. = $0.49 \text{ kcal mol}^{-1} \text{ HA}^{-1}$). With respect to the electronic nature of the coumarin ring, the dimethyl substitution as in compound **6** was preferred over the more electron rich (compound **7**) or electron deficient (compound **8**) coumarin analogs.

Next, we explored replacement of O1 of the coumarin ring with nitrogen to produce the 1,2-dihydroquinolin-2-one (DHQ) analogs **11-13**. This change was well tolerated, with 5,7-dimethyl-DHQ analog **13** ($K_i = 2.2 \mu\text{M}$; L.E. = $0.43 \text{ kcal mol}^{-1} \text{ HA}^{-1}$) essentially equipotent to its coumarin congener **6**. Substitution on the ring N atom in the DHQ scaffold was also tolerated, with analogs **11** and **12** exhibiting comparable potencies and ligand efficiencies. The favorable effect of C5/C7 substitution noted in the coumarin series is true as well in DHQ analogs, with dimethyl analog **13** notably more potent than unsubstituted DHQ comparators **11** and **12**. Quinoline analogs **14** and **15** lacking the ring carbonyl of the DHQ scaffold exhibited very weak potencies and ligand efficiencies 2–5 times inferior to the relevant DHQ comparator **11**, suggesting that the carbonyl group is involved in recognition and binding by KPC-2. Finally, the introduction of bromine substituents at C5 and C7 of the DHQ scaffold produced compound **16**, with activity ~7,000-fold improved over the parent DHQ analog **11**, and an impressive K_i of 20 nM against KPC-2 that is to our knowledge the highest affinity non-covalent inhibitor of any SBL reported to date.

To define key residues and interactions that contribute to inhibitor binding by KPC-2, we determined complex crystal structures with compounds **1**, **2**, **3**, **6**, and **9** (Fig. 1 and Fig. S2) at resolutions of 1.45 Å and better. All ligands were unambiguously identified in the composite simulated annealing $mF_o - DF_c$ omit maps contoured at 3σ . Interestingly, for the complex with compound **1**, there appears to be additional density corresponding to a potential second copy of **1**; however, the occupancy was too low to confidently model in. In each complex structure, the phosphonate moiety establishes hydrogen bonds (HB) with S70, S130, T235, T237, and forms a water-mediated HB with the backbone carbonyl of T216. Notably, the carbonyl oxygen atom of the inhibitor forms a water-mediated HB with R220 and H274, perhaps revealing why quinoline analogs **14** and **15** that lack such carbonyl functionality are weaker inhibitors of KPC-2.

Also revealed in these structures were some important details concerning the KPC-2 active site. The unfavorable effect of C6-Me substitution is explained by a potential steric clash between the C6 methyl group and N132, which restricts the binding mode of **1** (Fig. 1a). Moving this substituent to the C5 position as in **6** and **9** avoids the steric occlusion and allows the coumarin ring to swing towards W105 (Fig. 1b). Concomitantly, a conformational change in W105 brings the side chain closer to the face of the coumarin ring, forming a π - π stacking interaction. At the same time, the C5-Me substituent in compounds **6** and **9** itself contributes to binding affinity by forming non-polar interactions with W105. Regarding KPC-2 enzymology, the large hydrophobic surface of W105, coupled with a conformational flexibility revealed in our complex and apo structures (Fig. 1c, 1d), appears to endow KPC-2 with significant versatility in interacting with small molecule substrates and inhibitors.

The SAR analysis and complex crystal structures also highlight the contribution to ligand binding of a non-polar surface consisting of P104 and especially L167, which is in contact with the C7-Me or C7-Br substitutions in **6**, **9** and **16** (Fig. 1 and S2). Replacing the C7-Me in **9** by -Br in **16** increases the activity by ~12-fold, through increasing the interactions with this non-polar surface.

Cross-class inhibition of metallo- β -lactamases

Having established that heteroaryl phosphonates are recognized by the active site of KPC-2, we next asked whether the clinically relevant MBLs NDM-1 and VIM-2 might also recognize these compounds, as SBLs and MBLs clearly do with their shared β -lactam substrates²⁹. We first tested a subset of the coumarin, DHQ, and quinoline analogs for biochemical activity against NDM-1 and VIM-2. Notably, inhibition of NDM-1 and VIM-2 was generally strongest for analogs with substitution at both C5 and C7, mirroring our findings with KPC-2 (Table 1). Thus, compounds **6**, **8**, **9**, **13**, and **16** were better inhibitors of the MBLs than comparators lacking C5 and C7 substituents (**11**, **12**, **14**, **15**). Compounds **9** and **16**, the most potent KPC-2 inhibitors, were also two of the most potent inhibitors of NDM-1 ($K_i = 34.2 \mu\text{M}$ and $31.4 \mu\text{M}$) and VIM-2 ($K_i = 1.2 \mu\text{M}$ and $0.316 \mu\text{M}$). While the compounds inhibited VIM-2 more potently than NDM-1, rank-order activity of the compound series was similar for the two enzymes. Generally, and across all three enzymes, inhibitor potency improved with increasing hydrophobic surface area. There is a particularly striking correlation between the activities for KPC-2 and VIM-2 (Table 1, e.g. comparing **15**, **6** and **16**). However, compared with KPC-2, the MBLs were less sensitive to the positioning of ring substituents (e.g., C5 vs C6, comparing **1** and **6**). Ring fluorination as in analogs **8** and **10** was unexpectedly detrimental to NDM-1 activity, an observation that will require further investigation.

Complex structures were determined for NDM-1 with compounds **1-3**, **6-9**, and **11-14**, and for VIM-2 with compounds **8** and **14**, all solved at resolutions of 1.70 Å and better (Fig. 2, Fig. S3-S4), initially using soaking conditions at acidic pH (pH 3.8) to maintain stability of NDM-1 (vide infra). The binding orientation of the inhibitors was unambiguously identified in the composite simulated annealing mF_o-DF_c omit maps contoured at 3σ (Fig. 2, Fig. S3-S4). In each structure, the phosphonate group bridges the zinc ions in NDM-1 and VIM-2, displacing a hydroxide ion that is essential for catalysis⁴. For NDM-1, the coumarin, DHQ, and quinoline analogs all form common interactions within the active site. These interactions include HBs from the phosphonate group to N220 and D124, the latter of which forms a similar interaction with the hydroxide ion in apo structures^{30, 31}. The heteroaryl ring of all three scaffolds form non-polar interactions with M67, W93 and V73. An edge-face interaction between the heteroaryl ring and F70 is evident in many NDM-1 complex structures.

One interesting and unexpected aspect revealed in the NDM-1 structures is the ability of the enzyme to bind similar ligands in one of two distinct orientations: one pointing the ring carbonyl group away from V73 (pose 1, e.g., compound **1**, Fig. 2a) and the other towards it (pose 2, e.g., **6**, Fig. 2b). Pose 1 is observed in the complex structures of compounds lacking C5 substitution (e.g., **1**, Fig. 2 and **2**, **3**, **11**, **12** Fig. S3). In contrast, pose 2 is favored for

compounds with C5 substitutions as it allows additional interactions with H122 (e.g., pi-sigma interaction with -Me in **6** (distance 3.67 Å), Fig. 2b; pi-alkyl interaction with -Br in **9** (distance 3.78 Å), Fig. S3d). This small pocket near H122 in NDM-1 is analogous to the slot adjacent to W105 in KPC-2, which similarly accommodates the C5 substituent. Also, of note, is that the side chain of F70 in NDM-1 exhibits significant conformational mobility, allowing the formation of favorable CH- π interactions with the C7-Me of **1** (Fig. 2a) and edge-face interactions with compounds **11** and **12** (Fig. S3). Overall the relative openness of the NDM-1 active site and the flexibility of the M67-F70 loop accommodates distinct binding orientations depending on ligand substitution pattern³². To some extent this echoes the role of W105 in KPC-2 while affording more plasticity in ligand binding³³. However, as described earlier, KPC-2 is more sensitive than NDM-1 to the positions of the substituents on the heteroaryl ring, as demonstrated by the different activities of compounds **1** (C6/C7 substitution) and **6** (C5/C7 substitution) against KPC-2, in contrast to the similar K_i values against NDM-1.

We solved structures of the 5,7-difluoro compound **8** (Fig. 2) and the smaller quinoline analog **14** (Fig. S3) bound to both NDM-1 and VIM-2, also at pH 3.8, to compare how these two MBLs interacted with a common ligand. Although compound **8** did not show inhibition of NDM-1 under our standard experimental conditions, pre-incubation of the compound with NDM-1 demonstrated weak inhibitory activity (data not shown), suggesting the compound does interact with NDM-1. In both structures with NDM-1 and VIM-2, compound **8** adopts pose 2, with the phosphonate group forming a HB with N233 and D120 in VIM-2 (Fig. 2d). The coumarin ring of compound **8** forms a π - π stacking interaction with Y67 of VIM-2, van der Waals interactions with W87, and an edge-face interaction with H263, analogous to the contacts made by other analogs with F70/W93/H250 in NDM-1. Unique to VIM-2 is the presence of R228 near the active site, which can establish a HB with the carbonyl oxygen of compound **8** and may enhance binding and constrain the orientation of the compound, particularly in comparison to NDM-1. In addition, the stacking interactions between the inhibitor and Y67 in VIM-2 may be more favorable than contacts with similarly positioned residues M67 or F70 in NDM-1 and can also contribute to stronger binding affinity for VIM-2.

The observed displacement of the active site hydroxide by phosphonate-bearing inhibitors in the structures described above, together with the low pH of the soaks, suggested that the phosphonate group was in the protonated monoanionic state, and therefore was able to form a HB with the negatively charged D124, similar to the hydroxide. The use of these conditions was required as the WT NDM-1 crystals were only stable at low pH. We hypothesized that this was due to the need for a neutral/protonated D199 at the crystal packing interface. We subsequently constructed a D199N mutant and were able to determine the complex structures of **7** and **16** at physiological pH (pH 7.5) (Fig. 3), where the phosphonate group may also exist in the dianionic state, especially when in close proximity to the zinc ions. As posited, the complex structures at pH 7.5 retained the active site hydroxide. The phosphonate group in this case interacts with the hydroxide and one of the zinc ions (Zn2), rather than both zinc ions as in the low pH structures. As a result, there is a shift in the position of the phosphonate group, together with the rest of the inhibitor. This

movement was accompanied by different conformations of ligand-interacting residues such as M67 and F70. Comparing **16** (Fig. 3a) and the mono-bromo coumarin analog **9** (Fig. S3d), a flip of the heteroarene ring was also observed, allowing **16** to adopt a binding mode similar to pose 1 as described above (Fig. 2a). This is possibly due to the ability of the C5/C7 bromo substituents to establish favorable interactions with H250 and F70. Overall the complex structure at pH 7.5 provide detailed and valuable information for future lead optimization. But the lower pH structures, particularly with their well-defined electron densities, offer important insights into how active site flexibility enables NDM-1 to respond to changes in ligand/substrate structure including small changes in the ligand protonation states.

We also determined the complex crystal structure of VIM-2 with compound **16** at pH 7.5 (Fig. 4a, Fig. S4b). Unlike the complex structure with **8**, the carbonyl group is pointed away from R228 without forming a HB. One oxygen of the phosphonate group is positioned 3.7 Å from R228, suggesting favorable electrostatic interactions. The DHQ ring with the di-bromo substituents establishes extensive interactions with H263, R228, W87 and especially Y67 and F61. In addition, compared with NDM-1, the binding pocket is slightly narrower in VIM-2 with the loop of G232-N233 lowered closer to the ligand, and the planar peptide bond between G232 and N233 stacked on top of the DHQ ring (Fig. 4a). The new contacts with R228, G232 and N233, together with the favorable stacking interactions with Y67 and F61, may explain the ~100x higher affinity of **16** for VIM-2 than NDM-1. However, despite these differences, it is important to note that the overall binding orientation of **16** is similar between VIM-2 and NDM-1 (Fig. 4b), echoing the observations of the complex structures of **8** (Fig. 2), and demonstrating the feasibility of lead optimization simultaneously improving activity against both enzymes.

Cell-based activity of compounds **9**, **11**, **13** and **16**.

To investigate the effects of these inhibitors on bacterial cells, coumarin **9** and DHQ analogs **11** and **13** were tested (at fixed 128 µg/mL concentrations) in combination with the carbapenem antibiotic imipenem against Gram-negative clinical isolates known to produce carbapenemases (Table 2). Compound **9** restored susceptibility to imipenem in a *K. pneumoniae* strain producing KPC-2 and reduced the minimum inhibitory concentration (MIC) by 64-fold. It also decreased the MIC for imipenem by 4-fold in an NDM-1 producing *E. coli* strain and more than 2-fold in an NDM-1 producing *K. pneumoniae* strain. Compound **9** did not have any activity against NDM-1 producing *Enterobacter cloacae*. Compared to KPC-2, the relatively lower cell-based activity of **9** against NDM-1 expressing strains correlates with the different *in vitro* activities observed in biochemical testing. The DHQ analog **13** was comparable to compound **9**, reducing the MIC of imipenem by 64-fold in KPC-2 producing *K. pneumoniae* and 4-fold in NDM-1 producing *E. coli*, but unable to rescue imipenem activity in NDM-1 producing *K. pneumoniae/E. cloacae* or in VIM-2 producing *P. aeruginosa*. The variable susceptibility of the different bacterial strains likely reflects the influence of other resistance mechanisms such as active efflux. Consistent with its weaker biochemical activity, DHQ analog **11** was less effective than compounds **9** or **13** in reducing the MIC of imipenem against the KPC-2 producing *K. pneumoniae* and exhibited little if any effect against NDM-1 producing *E. coli*, *K. pneumoniae*, and *E.*

cloacae. In general, the microbiological studies revealed that heteroaryl phosphonate analogs can cross the outer membrane to target both serine and metallo-carbapenemases in Gram-negative bacteria, at least at high concentrations.

Following these initial experiments, we performed a more extensive microbiological assessment of the most potent DHQ analog **16** (Table 3). A checkerboard assay using a clinical KPC-2 expressing *K. pneumoniae* strain varied both imipenem and inhibitor concentrations and demonstrated that compound **16**, at 128 µg/mL, reduced the MIC of imipenem by 128-fold, and by 32-fold when applied at 16 µg/mL concentration. In comparison, at 16 µg/mL concentration, avibactam lowered the imipenem MIC by 512-fold to 1 µg/mL. These results illustrated the dose-dependent effect of compound **16**, while highlighting its activity at more therapeutically relevant concentrations. We also studied this compound (at a fixed concentration of 128 µg/mL) across a series of isogenic carbapenemase-expressing *P. aeruginosa* strains with deletion of the efflux pumps MexAB-OprM and MexXY-OprM, or over-expressing MexAB-OprM. For the strains lacking efflux pumps, the imipenem MIC was reduced by 32, 16, and 16-fold for KPC-2, NDM-1 and VIM-2, respectively. It should be noted that, for KPC-2 (strain 4135) and VIM-2 (strain 4882), the MIC of imipenem was 2 µg/mL in these experiments in the presence of compound **16**, the same as the MIC of imipenem alone in the control strain without any carbapenemase (strain 4173, Table 3). Thus, an MIC reduction of 32 and 16-fold is the maximum that we could observe for KPC-2 and VIM-2, respectively. For the strains overexpressing efflux pumps, the imipenem MIC was reduced by 4 and 8-fold for NDM-1 and VIM-2, respectively. Overall the MIC data in the presence of compound **16** mirror the inhibition results from the biochemical assays, consistent with the different activities against KPC-2, NDM-1, and VIM-2. Although overexpressing efflux pumps did decrease its potency by up to 4-fold against NDM-1, the inhibitor retained significant cell-based activity in these bacterial strains.

The cytotoxicity of the phosphonate compounds was also evaluated using compound **16** and human HEK 293T cells. Compound **16** showed cytotoxicity in these experiments only when used at concentrations of 100 µg/mL and above, with 88% cell recovery rate at 100 µg/mL and 70% recovery rate at 200 µg/mL (Fig. S5). In addition, without imipenem, neither **9** nor **16** showed any antibacterial effects by itself at 128 µg/mL. Although we used up to 128 µg/mL inhibitor concentrations in our MIC testing, compound **16** displayed significant cell-based activity at lower concentrations (e.g., reducing imipenem MIC by 32-fold at 16 µg/mL) that will be more relevant to clinical applications. Nevertheless the potential cytotoxicity of these inhibitors should be further characterized in future development given previous studies showing the adverse effects of the phosphono-alkylquinoline compounds³⁴.

To assess the drug-like properties of this new scaffold, compound **16** was evaluated in a small panel of standard in vitro ADME assays (Table 4). The compound exhibited excellent stability when incubated with mouse liver microsomes and also reasonably high solubility in pH 7.4 phosphate buffered saline (PBS). Perhaps on account of its anionic nature, **16** was poorly permeable across MDCK-MDR monolayers, predicting for low oral absorption and blood-brain barrier penetrance. Given that most β-lactam antibiotics used to treat serious

infections are administered parenterally, the *in vitro* ADME profile of **16** is quite satisfactory as a starting point for future *in vivo* proof-of-concept studies and lead optimization efforts.

Discussion

Antibiotic resistance conferred by SBLs and MBLs in Gram-negative pathogens is a serious threat to human health. We have identified and characterized the first series of non-electrophilic, cross-class inhibitors of SBLs and MBLs. The structures and SAR described here provide insights into inhibitor discovery against these important antibiotic targets by providing new leads, and by elucidating the structural features underlying the broad substrate spectrum of carbapenemases.

Non-covalent phosphonate compounds as cross-class inhibitors

Phosphonate-bearing fragments of modest affinity have been described previously for SBLs^{35, 36}, while inhibitors bearing electrophilic phosphonate esters have been studied as traditional suicide substrate inhibitors of SBLs by Pratt and colleagues^{37–40}. Mercaptophosphonates were found to inhibit MBLs in a non-covalent fashion; however, they possess no activity against SBLs⁴¹. In contrast, the inhibitors detailed herein bind both SBLs and MBLs through a reversible, non-covalent mechanism, as evidenced by their complex crystal structures and the absence of time-dependent inhibition kinetics. The role of the phosphonate function in these new compounds resides in its ability to mimic the carboxylate group of substrates, rather than as a reactive surrogate of the scissile bond in substrates, as in the case of activated phosphonate ester inhibitors. Their expanded spectrum of inhibition, novel reversible mechanism, and minimal cytotoxicity in mammalian cells, suggests (2-oxo-1,2-dihydroquinolin-4-yl)methyl phosphonates as a viable new scaffold for antibiotic development.

The emergence of MBLs in recent years has led to increasing interest in novel inhibitor development against these proteins and resulted in many promising lead scaffolds including some also containing phosphonate groups^{42–46}. Most of these compounds are not active against SBLs. A recently identified series of MBL inhibitors contain both carboxylate and phosphonate moieties, and it is the carboxylate rather than the phosphonate group that interacts with the zinc ions in the complex crystal structures⁴³. Bisphosphonate compounds have also been shown to inhibit both MBLs and SBLs, but the mode of action is not entirely clear for these compounds partially due to the lack of crystal structures⁴⁴. In addition, pre-incubation appeared to significantly increase these compounds' potency against SBLs, suggesting they may function as covalent inhibitors.

Whereas most inhibitor development efforts have focused on either SBLs^{47–57} or MBLs^{18, 43, 45, 46, 58–62}, there have been some early successes of cross-class inhibitors^{44, 63}, most notably the cyclobutanone analogs of β -lactam antibiotics^{64, 65}. The recently developed cyclic-boronate esters represent arguably the most promising broad-spectrum inhibitors targeting both SBLs and MBLs²⁴. One such inhibitor, named VNRX-5133, has demonstrated promising activity in clinical trials against SBL and MBL producing Gram-negative bacteria⁶⁶. Essentially, these cyclic-boronates function as covalent transition state analogs in the case of SBLs, and paradoxically as non-covalent inhibitors of MBLs. By

contrast, the compounds described herein are to our knowledge the highest affinity cross-class inhibitors with a shared, reversible mode of non-covalent inhibition for both SBLs and MBLs. Importantly, these inhibitors capture functionally equivalent structural features of both SBLs and MBLs, with the phosphonate moiety placed in the subpocket recognizing the carboxylate of substrate in both classes of enzymes (Fig. 5) and highlighting the potential to further improve activity simultaneously against both serine- and metallo-enzymes. In KPC-2, this sub-pocket consists of S130, T235, and T237⁶⁷. In NDM-1/VIM-2, one of the two zinc ions and neighboring residues play a similar role in recognizing the same substrate C3'/4' carboxylate group^{4, 16}. The phosphonate group serves as an anchor that situates the compound similarly in KPC-2 and NDM-1/VIM-2 relative to substrate binding.

Accordingly, inhibitors positioned in this way form similar interactions with other conserved active site features in both SBLs and MBLs that recognize the same substrate functional groups, such as W105 in KPC2 and W93/M67 in NDM-1 that interact with the conjugated 5/6-membered ring of the β -lactam (Fig. 1, 3, 5). Such similarities in ligand binding features are underscored by the correlation between the inhibitors' activities for KPC-2, NDM-1 and VIM-2, as the hydrophobic surface area of the inhibitor increases (Table 1). Meanwhile, the potency of the inhibitors was consistently >10-fold weaker against NDM-1 than for KPC-2 or VIM-2, suggesting further subtleties of compound binding/inhibition that will need to be understood and exploited as these compounds are optimized towards more advanced lead compounds, which is the focus of our continuing efforts. Compared with β -lactam substrates, the current inhibitors engage only those active site surfaces that bind the core β -lactam structure – the fused bicycle and the C3'/4' carboxylate group – leaving largely unexplored the residues interacting with distal side chains (e.g., the amino-benzyl group of ampicillin, Fig. 5b). Targeting these additional ligand binding hot spots is expected to further improve potencies against NDM-1 as well as against the other carbapenemases. It should also be mentioned that our current inhibitors showed no activity against OXA-48 Class D carbapenemase (data not shown), possibly due to a narrower active site of Class D β -lactamases that may require a smaller core heterocycle for effective inhibition. Nonetheless the heteroaryl phosphonate scaffold can be engineered to target a wide range of carbapenemases due to the need of these enzymes to recognize the same substrates.

Structural basis for carbapenemase broad-spectrum substrate profile

The novel inhibitors and complex crystal structures described here also shed light on particular aspects of carbapenemase substrate recognition that add to our understanding of these enzymes' broad-spectrum activity and that will be useful for future antibiotic development. The new complex structures reveal the contributions of several hydrophobic residues to ligand binding, notably W105/L167 in KPC-2, Y67/W87 in VIM-2, and M67/F70/V73/W93 in NDM-1. The conformational flexibility of specific residues like W105 in KPC-2, F70 in NDM-1, and Y67/R228 in VIM-2 moreover provide important adaptability in the recognition of small molecules. Thus, in KPC-2 we uncovered multiple W105 conformations in binding of compounds **1** and **6**, a mobility rarely observed in the analogous residue Y105 of other Class A SBLs^{33, 68–70}. Likewise, residue F70 and the surrounding loop in NDM-1 is observed in our structures in distinct conformations depending on ligand structure. In VIM-2, R228 adopts different conformations upon binding to compounds **8** and **14**, making important HBs in both cases. The adaptability of MBLs is

also revealed in the two different ligand conformations (poses 1 and 2) we observed in the complex structures of NDM-1 (e.g., **1** vs **6**, Fig. 2a, b), resulting partially from the relative openness of the MBL active sites. Together, these features endow carbapenemases with a ligand binding versatility that may underlie their ability to hydrolyze a wide variety of β -lactam antibiotics but paradoxically may also enable and facilitate new inhibitor discovery^{14, 67}. The susceptibility to small molecule inhibition is highlighted by the remarkable L.E. of compound **16** against KPC-2 (0.59 kcal mol⁻¹ HA⁻¹), demonstrating the feasibility of using non-covalent inhibitors to achieve potent activity against carbapenemases. In addition, the ligand binding versatility of carbapenemases is also demonstrated by the observation of multiple copies of some inhibitors in the active site (e.g., compound **8** in VIM-2, Fig. S3), even though some of them were left unmodeled due to low occupancy (e.g., compound **1** in KPC-2).

Conclusion

In summary, we have presented herein multiple heteroaryl phosphonate scaffolds with cell-based activity, low-nM to low- μ M biochemical activities against both SBLs and MBLs, and with favorably lead-like physiochemical properties (clogD, solubility) and *in vitro* ADME properties. As such, this new scaffold appears quite suitable for further carbapenemase inhibitor discovery efforts. To support such efforts more broadly, we have detailed new structural information that enhances current understanding of carbapenemase activity and spectrum, reveals the structural basis for ligand/substrate binding, and should help guide drug discovery efforts aimed at better addressing the most intractable of Gram-negative bacterial infections.

Experimental Section

Compound Synthesis

Compounds **1–6** were obtained from commercial sources while compounds **7–15** were synthesized as detailed below. All synthetic analogs submitted for biochemical or biological testing were judged to be \geq 95% pure based on inspection of LC/MS and ¹H NMR spectra. Scans of representative ¹H NMR spectra are provided in the Supporting Information. ¹H and ¹³C NMR spectra were recorded on Varian INOVA-400 400 MHz and Bruker 500 MHz spectrometers. Chemical shifts are reported in δ units (ppm). NMR spectra were referenced relative to residual NMR solvent peaks. Coupling constants (*J*) are reported in hertz (Hz). Air and/or moisture sensitive reactions were carried out under an argon atmosphere in oven-dried glassware using anhydrous solvents from commercial suppliers. Air and/or moisture sensitive reagents were transferred via syringe or cannula and were introduced into reaction vessels through rubber septa. Solvent removal was accomplished with a rotary evaporator at ca. 10–50 Torr. Column chromatography was carried out using a Biotage SP1 flash chromatography system and silica gel cartridges from Silicycle. Analytical TLC plates from EM Science (Silica Gel 60 F₂₅₄) were employed for TLC analyses. Mass analyses and compound purity were determined using Waters Micromass ZQTM, equipped with Waters 2795 Separation Module, Waters 2996 Photodiode Array Detector, and Waters 2424 ELS detector. Separations were carried out with an XTerra® MS C18, 5 μ m, 4.6 \times 50 mm column,

at ambient temperature (unregulated) using a mobile phase of water-methanol containing a constant 0.10 % formic acid. Fluorescence and absorbance data was collected on a Molecular Devices Flex Station 3.

[(5-methoxy-7-methyl-2-oxo-2H-chromen-4-yl)methyl]phosphonic acid (7)

Step 1. A mixture of ethyl 4-bromoacetoacetate (0.66 mL, 4.8 mmol) and triethyl phosphite (0.818 mL, 4.8 mmol) were stirred at 100 °C for 25 min in a microwave reactor. Purification by flash column chromatography (50% EA/hexanes followed by 100% EA) yielded 380 mg (30%) of ethyl 4-(diethoxyphosphoryl)-3-oxobutanoate as a pale yellow oil. ¹H NMR (400 MHz, CDCl₃) δ 4.18–4.06 (m, 6H), 3.61 (s, 2H), 3.24 (s, 1H), 3.19 (s, 1H), 1.35–1.20 (m, 9H). Step 2. To a cooled (0 °C) mixture of 5-methylresorcinol (0.12 g, 0.94 mmol) and ethyl 4-(diethoxyphosphoryl)-3-oxobutanoate (0.25 g, 0.94 mmol), was added concentrated sulfuric acid (0.25 mL). The reaction mixture was stirred at ambient temperature for 18 h. The reaction mixture was then poured into cold water. The precipitate formed was filtered and dried to obtain about 0.23 g of crude 4-diethyl [(5-hydroxy-7-methyl-2-oxo-2H-chromen-4-yl)methyl]phosphonate as a pale pink solid that was used without further purification in the next step. ¹H NMR (400 MHz, CDCl₃) δ 6.56 (s, 1H), 6.32 (s, 1H), 6.05 (s, 1H), 4.19–4.12 (m, 4H), 3.79 (s, 1H), 3.73 (s, 1H), 2.12 (s, 3H), 1.33 (br. t, *J* = 7.02 Hz, 6H). LC-MS: *m/z* = 327 [M+H]⁺. Step 3. To a solution of diethyl [(5-hydroxy-7-methyl-2-oxo-2H-chromen-4-yl)methyl]phosphonate (0.036 g, 0.1 mmol) in methanol (1 mL), was added (trimethylsilyl)diazomethane (1.1 mL, 2.2 mmol). The mixture was stirred at ambient temperature for 18 h, concentrated and isolated by flash column chromatography (12 g, 5% methanol/dichloromethane) to obtain about 36 mg (96%) of diethyl [(5-methoxy-7-methyl-2-oxo-2H-chromen-4-yl)methyl]phosphonate as a yellow solid. ¹H NMR (400 MHz, CDCl₃) δ 6.76 (s, 1H), 6.57 (s, 1H), 6.14 (s, 1H), 4.21–3.96 (m, 2H), 3.93 (s, 3H), 3.89–3.67 (m, 4H), 2.40 (s, 3H), 1.44–1.17 (m, 6H) ¹³C NMR (100 MHz, CDCl₃) δ 160.25, 157.40, 155.33, 147.66, 147.56, 143.58, 115.43, 115.35, 110.55, 107.71, 62.49, 62.42, 55.97, 52.74, 52.68, 34.38, 33.02, 22.02, 16.41, 16.35. LC-MS: *m/z* = 341 [M+H]⁺. Step 4. A mixture of diethyl [(5-methoxy-7-methyl-2-oxo-2H-chromen-4-yl)methyl]phosphonate (0.036 g, 0.1 mmol) and 4 M solution of hydrochloric acid in dioxane (1 mL) were stirred at 100 °C for 48 h. The reaction mixture was concentrated down to dryness azeotropically with toluene, washed with ethyl acetate to obtain 23 mg of compound **7** (77%) as a tan solid. ¹H NMR (400 MHz, CD₃OD) δ 6.78 (s, 2H), 6.18 (d, *J* = 4.7 Hz, 1H), 3.96 (s, 3H), 3.78 (s, 1H), 3.72 (s, 1H), 2.43 (s, 3H). ¹³C NMR (100 MHz, CD₃OD) δ 161.22, 158.01, 155.13, 150.34, 150.24, 144.02, 114.10, 114.01, 109.47, 107.98, 107.32, 55.26, 35.34, 34.04, 20.49. LC-MS: *m/z* = 285 [M+H]⁺.

[(5,7-difluoro-2-oxo-2H-chromen-4-yl)methyl]phosphonic acid (8)

Step 1. To a cooled (0 °C) mixture of ethyl 4-bromoacetoacetate (0.26 mL, 1.9 mmol) in concentrated sulfuric acid (0.5 mL), was added 3, 5-difluorophenol (0.25 g, 1.9 mmol). The reaction mixture was stirred at ambient temperature for 18 h. Reaction mixture was then diluted with cold water and extracted with ethyl acetate. The organic extracts were washed with saturated aqueous sodium bicarbonate solution, brine, dried over magnesium sulfate and purified by flash column chromatography (35% ethyl acetate/hexanes) to obtain 150 mg (28%) of 4-(bromomethyl)-5,7-difluoro-2H-chromen-2-one as a white solid. ¹H NMR (400

MHz, CDCl₃) δ 6.99–6.93 (m, 1H), 6.90–6.82 (m, 1H), 6.50 (s, 1H), 4.60 (d, *J* = 2.2 Hz, 2H). LC-MS: *m/z* = 275 [M+H]⁺. Step 2. A mixture of 4-(bromomethyl)-5,7-difluoro-2H-chromen-2-one (0.038 g, 0.1 mmol) and triethyl phosphite (0.047 mL, 0.3 mmol) were heated to 100 °C for 18 h. The reaction mixture was purified by flash column chromatography (50% ethyl acetate/hexanes followed by 5% methanol/dichloromethane) to obtain 15 mg (33%) of the title compound as a pale yellow solid. ¹H NMR (400 MHz, CDCl₃) δ 6.93 (dt, *J* = 8.5, 1.9 Hz, 1H), 6.88–6.75 (m, 1H), 6.31 (d, *J* = 4.9 Hz, 1H), 4.14 (quin, *J* = 7.4 Hz, 4H), 3.51 (s, 1H), 3.45 (s, 1H), 1.30 (t, *J* = 7.1 Hz, 6H). LC-MS: *m/z* = 333 [M+H]⁺. Step 3. A mixture of diethyl [(5,7-difluoro-2-oxo-2H-chromen-4-yl)methyl]phosphonate (0.014 g, 0.0 mmol) and 4 M solution of hydrochloric acid in dioxane (1 mL) were stirred at 100 °C for 48 h. The reaction mixture was concentrated down to dryness azeotropically with toluene, washed with 50% ethyl acetate /hexanes to obtain 11 mg of compound **8** (95%) as a tan solid. ¹H NMR (400 MHz, CD₃OD) δ 7.15–6.98 (m, 2H), 6.38 (d, *J* = 4.9 Hz, 1H), 3.57 (s, 1H), 3.51 (s, 1H), LC-MS: *m/z* = 277 [M+H]⁺.

Synthesis of [(5-bromo-7-methyl-2-oxo-2H-chromen-4-yl)methyl]phosphonic acid (**9**)

Step 1. To a cooled (0 °C) mixture of 3-bromo-5-methylphenol (0.400 g, 2.1 mmol) and concentrated sulfuric acid (0.5 mL), was added ethyl 4-bromoacetoacetate (0.296 mL, 2.1 mmol) slowly. The reaction mixture was stirred at ambient temperature for 18 h. Reaction mixture was then diluted with cold water and extracted with ethyl acetate. The organic extracts were washed with brine, dried over magnesium sulfate and purified by flash column chromatography (0–25% ethyl acetate/hexanes) to obtain 134 mg (24%) of 5-bromo-4-(bromomethyl)-7-methyl-2H-chromen-2-one as a cream colored solid. ¹H NMR (400 MHz, CDCl₃) δ 7.46 (s, 1H), 7.17 (s, 1H), 6.61 (s, 1H), 5.00 (s, 2H), 2.42 (s, 3H). LC-MS: *m/z* = 332 [M+H, ⁷⁹Br]⁺, 334 [M+H, ⁸¹Br]⁺. Step 2. A mixture of 5-bromo-4-(bromomethyl)-7-methyl-2H-chromen-2-one (0.130 g, 0.4 mmol) and triethyl phosphite (0.134 mL, 0.8 mmol) were stirred in at 100 °C for 24 h. The reaction mixture was diluted with ethyl acetate and washed with water and brine. The organic layer was dried over magnesium sulfate and purified by flash column chromatography (0–50% ethyl acetate/hexanes) to obtain 90 mg (59%) of diethyl [(5-bromo-7-methyl-2-oxo-2H-chromen-4-yl)methyl]phosphonate as a yellow oil that solidifies on standing. ¹H NMR (400 MHz, CDCl₃) δ 7.44 (s, 1H), 7.15 (s, 1H), 6.44 (d, *J* = 4.8 Hz, 1H), 4.24–4.08 (m, 4H), 4.06 (s, 1H), 4.00 (s, 1H), 2.41 (s, 3H), 1.28 (t, *J* = 7.0 Hz, 6H). ¹³C NMR (100 MHz, CDCl₃) δ 158.92, 158.89, 155.46, 147.33, 143.12, 133.20, 119.44, 119.00, 118.90, 118.08, 115.70, 62.65, 62.59, 55.97, 33.66, 32.29, 16.39, 16.33. LC-MS: *m/z* = 388 [M+H, ⁷⁹Br]⁺, 390 [M+H, ⁸¹Br]⁺. Step 3. A mixture of diethyl [(5-bromo-7-methyl-2-oxo-2H-chromen-4-yl)methyl]phosphonate (0.090 g, 0.2 mmol) and 4 M solution of hydrochloric acid in dioxane (0.6 mL) were stirred at 100 °C for 24 h. The reaction mixture was concentrated, washed with ethyl acetate and dried to obtain 70 mg (91%) of compound **9** as a tan powder. ¹H NMR (400 MHz, *d6*-DMSO) δ 7.53 (s, 1H), 7.29 (s, 1H), 6.44 (d, *J* = 4.5 Hz, 1H), 3.91 (s, 1H), 3.84 (s, 1H), 2.37 (s, 3H). ¹³C NMR (100 MHz, *d6*-DMSO) δ 156.56, 155.31, 149.40, 149.31, 143.46, 133.13, 119.39, 118.90, 118.06, 117.97, 117.46, 115.75, 115.71, 34.17, 32.85, 19.37. LC-MS: *m/z* = 332 [M+H, ⁷⁹Br]⁺, 334 [M+H, ⁸¹Br]⁺.

[(5-fluoro-7-methyl-2-oxo-2H-chromen-4-yl)methyl]phosphonic acid (10)

Step 1. To a cooled (0 °C) mixture of 3-fluoro-5-methylphenol (0.200 g, 1.6 mmol) and ethyl 4-bromoacetoacetate (0.219 mL, 1.6 mmol), was added concentrated sulfuric acid (0.8 mL). The reaction mixture was stirred at ambient temperature for 18 h. Reaction mixture was then diluted with cold water and extracted with ethyl acetate. The organic extracts were washed with brine, dried over magnesium sulfate and concentrated *in vacuo* to obtain 0.23 g of the crude 4-(bromomethyl)-5-fluoro-7-methyl-2H-chromen-2-one as a pale yellow solid which was used without further purification. Step 2. A mixture of 4-(bromomethyl)-5-fluoro-7-methyl-2H-chromen-2-one (0.200 g, 0.7 mmol) and triethyl phosphite (0.253 mL, 1.5 mmol) were stirred at 100 °C for 18 h. The reaction mixture purified by flash column chromatography (50% ethyl acetate/hexanes followed by 100% ethyl acetate) to obtain 155 mg (64%) of diethyl [(5-fluoro-7-methyl-2-oxo-2H-chromen-4-yl)methyl]phosphonate as a pale yellow oil. ¹H NMR (400 MHz, CDCl₃) δ 6.98 (s, 1H), 6.84 (d, *J* = 12.9 Hz, 1H), 6.44 (d, *J* = 4.8 Hz, 1H), 4.20–4.03 (m, 4H), 3.52 (s, 1H), 3.46 (s, 1H), 2.43 (s, 3H), 1.36–1.22 (m, 6H). LC-MS: *m/z* = 329 [M+H]⁺. Step 3. A mixture of diethyl [(5-fluoro-7-methyl-2-oxo-2H-chromen-4-yl)methyl]phosphonate (0.026 g, 0.1 mmol) and 4 M solution of hydrochloric acid in dioxane (1 mL) were stirred at 100 °C for 18 h. The reaction mixture was concentrated and purified by reverse phase HPLC to obtain 16 mg (74%) of compound **10** as a white solid. ¹H NMR (400 MHz, CD₃OD) δ 7.06 (s, 1H), 6.98 (d, *J* = 13.1 Hz, 1H), 6.35 (d, *J* = 4.8 Hz, 1H), 3.56 (s, 1H), 3.51 (s, 1H), 2.45 (s, 3H). ¹³C NMR (125 MHz, *d6*-DMSO) δ 160.33, 159.37, 158.31, 154.38, 148.39, 148.31, 144.17, 144.08, 116.21, 113.61, 113.11, 112.93, 107.37, 107.28, 35.57, 34.66, 34.57, 21.39 LC-MS: *m/z* = 273 [M+H]⁺.

[(2-oxo-1,2-dihydroquinolin-4-yl)methyl]phosphonic acid (11)

Step 1. A mixture of 4-bromomethyl-2(1H)-quinolinone (0.500 g, 2.1 mmol) and triethyl phosphite (0.720 ml, 4.2 mmol) were heated in dioxane (2 mL) to 100 °C for 18 h. The reaction mixture was concentrated and purified by flash column chromatography (0–5% methanol/dichloromethane) to obtain 300 mg (48%) of diethyl [(2-oxo-1,2-dihydroquinolin-4-yl)methyl]phosphonate as cream colored solid. ¹H NMR (400 MHz, CDCl₃) δ 12.82 (br.s, 1H), 7.82 (d, *J* = 8.2 Hz, 1H), 7.39–7.57 (m, 2H), 7.25–7.23 (m, 1H), 6.72 (d, *J* = 3.9 Hz, 1H), 4.07 (quin, *J* = 7.3 Hz, 4H), 3.46 (s, 1H), 3.40 (s, 1H), 1.25 (t, *J* = 7.0 Hz, 6H) LC-MS: *m/z* = 296 [M+H]⁺. Step 2. A mixture of diethyl [(2-oxo-1,2-dihydroquinolin-4-yl)methyl]phosphonate (0.025 g, 0.085 mmol) and 4 M solution of hydrochloric acid in dioxane (1 mL) were stirred at 100 °C for 24 h. The reaction mixture was concentrated down to dryness purified by reverse phase HPLC to obtain 11 mg (54%) of compound **11** as a white solid. ¹H NMR (400 MHz, *d6*-DMSO) δ 11.64 (br.s, 1H), 7.84 (d, *J* = 7.9 Hz, 1H), 7.46 (t, *J* = 7.4 Hz, 1H), 7.28 (d, *J* = 8.1 Hz, 1H), 7.15 (t, *J* = 7.4 Hz, 1H), 6.43 (d, *J* = 4.0 Hz, 1H), 3.26 (s, 1H), 3.19 (s, 1H). ¹³C NMR (100 MHz, *d6*-DMSO) δ 161.89, 145.71, 145.63, 139.29, 130.51, 126.49, 122.17, 121.76, 119.60, 115.72, 33.21, 31.94. LC-MS: *m/z* = 240 [M+H]⁺.

[(1-methyl-2-oxo-1,2-dihydroquinolin-4-yl)methyl]phosphonic acid (12)

Step 1. To a cooled (0 °C) solution of diethyl [(2-oxo-1,2-dihydroquinolin-4-yl)methyl]phosphonate (0.050 g, 0.2 mmol) in DMF (0.5 mL), was added sodium hydride,

60% (0.004 g, 0.2 mmol) and iodomethane (0.032 mL, 0.5 mmol). The mixture was stirred at ambient temperature for 2 h. The reaction mixture was then quenched with aqueous saturated ammonium chloride solution, extracted with ethyl acetate, washed with water and brine. The organic layer was dried over magnesium sulfate and purified by flash column chromatography (0–10% methanol/dichloromethane) to obtain 24 mg (46%) of diethyl [(1-methyl-2-oxo-1,2-dihydroquinolin-4-yl)methyl]phosphonate as a clear oil. ¹H NMR (400 MHz, CDCl₃) δ 7.87 (d, *J* = 7.6 Hz, 1H), 7.59 (t, *J* = 7.2 Hz, 1H), 7.39 (d, *J* = 8.5 Hz, 1H), 7.33–7.26 (m, 1H), 6.72 (d, *J* = 4.4 Hz, 1H), 4.11–4.04 (m, 4H), 3.72 (s, 3H), 3.40 (s, 1H), 3.35 (s, 1H), 1.28–1.24 (m, 6H). LC-MS: *m/z* = 310 [M+H]⁺. Step 2. A mixture of diethyl [(1-methyl-2-oxo-1,2-dihydroquinolin-4-yl)methyl]phosphonate (0.023 g, 0.1 mmol) and 4 M solution of hydrochloric acid in dioxane (2 mL) were stirred at 100 °C for 24 h. The reaction mixture was concentrated down to dryness and isolated by reverse phase HPLC to obtain 7 mg (37%) of the product as a white powder. ¹H NMR (400 MHz, *d*₆-DMSO) δ 7.93 (d, *J* = 7.9 Hz, 1H), 7.63–7.59 (m, 1H), 7.51 (d, *J* = 8.4 Hz, 1H), 7.26 (t, *J* = 7.4 Hz, 1H), 6.54 (d, *J* = 3.5 Hz, 1H), 3.62 (s, 3H), 3.26 (s, 1H), 3.20 (s, 1H). ¹³C NMR (100 MHz, *d*₆-DMSO) δ 161.03, 144.42, 144.33, 140.11, 130.97, 127.17, 122.14, 121.92, 120.54, 115.07, 33.17, 31.87, 29.33. LC-MS: *m/z* = 254 [M+H]⁺.

[(5,7-dimethyl-2-oxo-1,2-dihydroquinolin-4-yl)methyl]phosphonic acid (13)

Step 1. A mixture of 3,5-dimethylaniline (0.514 mL, 4.1 mmol), ethyl acetoacetate (1.043 mL, 8.2 mmol) and potassium tert-butoxide (0.046 g, 0.4 mmol) were stirred at 120 °C for 18 h. The reaction mixture was diluted with ethyl acetate, washed with aqueous saturated ammonium chloride, water and brine. The organic layer was dried over magnesium sulfate, concentrated and purified by flash column chromatography (35% ethyl acetate /hexanes) to obtain 0.33 g (39%) of N-(3,5-dimethylphenyl)-3-oxobutanamide as a yellow solid. ¹H NMR (400 MHz, CDCl₃) δ 9.06 (br.s, 1H), 7.18 (s, 2H), 6.77 (s, 1H), 3.55 (s, 2H), 2.30–2.20 (m, 9H). LC-MS: *m/z* = 206 [M+H]⁺. Step 2. To a mixture of N-(3,5-dimethylphenyl)-3-oxobutanamide (0.200 g, 1.0 mmol) in EtOAc (2 mL), was added pyridinium bromide perbromide (0.156 g, 0.5 mmol). The mixture was stirred at ambient temperature for an hour. The reaction mixture was concentrated in vacuo and purified by flash column chromatography (0–25% ethyl acetate /hexanes) to obtain 88 mg (32%) of 4-bromo-N-(3,5-dimethylphenyl)-3-oxobutanamide. Concentrated sulfuric acid (0.2 mL) was added to a cooled (0 °C) 4-bromo-N-(3,5-dimethylphenyl)-3-oxobutanamide (0.088 g, 0.31 mmol). The mixture was stirred at 40 °C for 18 h. Reaction mixture was then diluted with cold water and extracted with 5% methanol in dichloromethane. The organic extracts were washed with brine, dried over magnesium sulfate and concentrated *in vacuo* to obtain 68 mg of the crude 4-(bromomethyl)-5,7-dimethyl-1,2-dihydroquinolin-2-one as a cream solid which was used without further purification. ¹H NMR (400 MHz, CDCl₃) δ 12.48 (br.s, 1H), 7.17 (s, 1H), 6.92 (s, 1H), 6.74 (s, 1H), 4.77 (s, 2H), 2.91 (s, 3H), 2.43 (s, 3H). LC-MS: *m/z* = 265 [M+H, ⁷⁹Br]⁺, 267 [M+H, ⁸¹Br]⁺. Step 3. A mixture of 4-(bromomethyl)-5,7-dimethyl-1,2-dihydroquinolin-2-one (0.033 g, 0.12 mmol) and triethyl phosphite (0.17 mL, 0.96 mmol) was stirred in dioxane (2.0 mL) at 100 °C for 22 h. The reaction mixture was concentrated and purified by flash column chromatography (0–10% methanol/dichloromethane) to obtain 23 mg (57%) of diethyl [(5,7-dimethyl-2-oxo-1,2-dihydroquinolin-4-yl)methyl]phosphonate as a white solid. ¹H NMR (400 MHz, CDCl₃) δ

12.49 (br.s, 1H), 7.14 (s, 1H), 6.86 (s, 1H), 6.64 (d, $J=4.6$ Hz, 1H), 4.15–4.00 (m, 4H), 3.71 (s, 1H), 3.65 (s, 1H), 2.87 (s, 3H), 2.39 (s, 3H), 1.32–1.18 (m, 6H). LC-MS: $m/z = 324$ [M+H]⁺. Step 4. A mixture of diethyl [(5,7-dimethyl-2-oxo-1,2-dihydroquinolin-4-yl)methyl]phosphonate (0.023 g, 0.07 mmol) and 4 M solution of hydrochloric acid in dioxane (0.8 mL) were stirred at 100 °C for 24 h. The reaction mixture was concentrated down to dryness, purified by reverse phase HPLC to obtain 7 mg (37%) of compound **13** as a white solid. ¹H NMR (400 MHz, *d6*-DMSO) δ 11.54 (br.s, 1H), 6.92 (s, 1H), 6.76 (s, 1H), 6.28 (br.s, 1H), 3.42–3.36 (m, 2H), 2.78 (s, 3H), 2.25 (s, 3H) ¹³C NMR (100 MHz, *d6*-DMSO) δ 161.15, 141.06, 139.57, 136.60, 128.18, 123.65, 117.01, 116.98, 114.89, 36.58, 35.31, 25.02, 21.19. LC-MS: $m/z = 268$ [M+H]⁺.

[(quinolin-8-yl)methyl]phosphonic acid (**14**)

Step 1. A mixture of 8-(bromomethyl)quinoline (0.10 g, 0.5 mmol) and triethyl phosphite (0.154 mL, 0.9 mmol) were heated to 100 °C for 24h. The crude reaction mixture was subjected to flash column chromatography (50% ethyl acetate/hexanes followed by 5% methanol/dichloromethane) to obtain 40 mg (32%) of diethyl [(quinolin-8-yl)methyl]phosphonate as a clear oil. ¹H NMR (400 MHz, CDCl₃) δ 8.95 (d, $J = 3.8$ Hz, 1H), 8.16 (d, $J = 8.2$ Hz, 1H), 7.87 (dd, $J = 6.5, 3.5$ Hz, 1H), 7.75 (d, $J = 8.0$ Hz, 1H), 7.58–7.49 (m, 1H), 7.42 (dd, $J = 8.0, 4.1$ Hz, 1H), 4.13–3.91 (m, 6H), 1.21–1.07 (m, 6H). LC-MS: $m/z = 280$ [M+H]⁺. Step 2. A mixture of diethyl [(quinolin-8-yl)methyl]phosphonate (0.041 g, 0.1 mmol) and a 4 M solution of hydrochloric acid in dioxane (2 mL) were stirred at 100 °C for 24h. The reaction mixture was concentrated down to dryness azeotropically with toluene, washed with ethyl acetate and dried to obtain 37 mg (97%) of the title compound as HCl salt and white powder. ¹H NMR (400 MHz, *d6*-DMSO) δ 9.06 (dd, $J = 4.5, 1.6$ Hz, 1H), 8.67 (d, $J = 8.3$ Hz, 1H), 8.00 (d, $J = 8.3$ Hz, 1H), 7.92–7.87 (m, 1H), 7.67–7.78 (m, 2H), 3.78 (s, 1H), 3.73 (s, 1H). ¹³C NMR (100 MHz, *d6*-DMSO) δ 147.51, 143.58, 140.57, 134.61, 134.54, 129.90, 129.81, 129.26, 128.61, 127.75, 122.10, 31.28, 29.98. LC-MS: $m/z = 224$ [M+H]⁺.

[(quinolin-4-yl)methyl]phosphonic acid (**15**)

Step 1. To a mixture of triethyl phosphite (0.162 mL, 0.9 mmol) and zinc iodide (0.150 g, 0.5 mmol) in THF (1.5 mL), was added quinolin-4-ylmethanol (0.050 g, 0.3 mmol). The reaction mixture was stirred at 70 °C for 72 h. The mixture was then diluted with ethyl acetate, washed with aqueous saturated sodium bicarbonate solution, water and brine. The organic layer was dried over magnesium sulfate, concentrated and purified by reverse phase HPLC to obtain 9.5 mg (11%) of diethyl [(quinolin-4-yl)methyl]phosphonate as colorless oil. ¹H NMR (400 MHz, CD₃OD) δ 8.80 (d, $J = 4.6$ Hz, 1H), 8.28 (d, $J = 8.5$ Hz, 1H), 8.07 (d, $J = 8.5$ Hz, 1H), 7.82 (t, $J = 7.7$ Hz, 1H), 7.70 (t, $J = 7.7$ Hz, 1H), 7.56 (t, $J = 4.1$ Hz, 1H), 4.15–3.96 (m, 4H), 3.90 (s, 1H), 3.85 (s, 1H), 1.22 (t, $J = 7.1$ Hz, 6H). LC-MS: $m/z = 280$ [M+H]⁺. Step 2. A mixture of diethyl [(quinolin-4-yl)methyl]phosphonate (0.009 g, 0.032 mmol) and a 4 M solution of hydrochloric acid in dioxane (0.5 mL) were stirred at 100 °C for 18 h. The reaction mixture was concentrated down to dryness to obtain 8 mg (96%) of the title compound as a hydrochloride salt, as a white hygroscopic solid. ¹H NMR (400 MHz, CD₃OD) δ 9.13 (d, $J = 5.8$ Hz, 1H), 8.64 (d, $J = 8.8$ Hz, 1H), 8.28–8.16 (m, 2H), 8.14–7.99 (m, 2H), 4.10 (s, 1H), 4.04 (s, 1H). LC-MS: $m/z = 224$ [M+H]⁺.

[(5,7-dibromo-2-oxo-1,2-dihydroquinolin-4-yl)methyl]phosphonic acid (16)

Step 1. A mixture of 3,5-dibromolaniline (0.5 g, 2.0 mmol), ethyl acetoacetate (0.5 mL, 4.0 mmol) and potassium tert-butoxide (0.022 g, 0.2 mmol) were stirred at 120 °C for 24 h. The reaction mixture was diluted with ethyl acetate, washed with water and brine. The organic layer was dried over magnesium sulfate, concentrated and purified by flash column chromatography (35% ethyl acetate /hexanes) to obtain 0.1 g (15%) of N-(3,5-dibromophenyl)-3-oxobutanamide as a brown oil. ¹H NMR (400 MHz, CDCl₃) δ 9.40 (s, 1H), 7.74 (s, 2H), 7.43 (s, 1H), 3.62 (s, 2H), 2.55 (s, 3H). Step 2. To a mixture of N-(3,5-dibromophenyl)-3-oxobutanamide (0.090 g, 0.3 mmol) in acetic acid (0.2 mL), bromine (0.015 mL, 0.3 mmol) was added slowly. After stirring at room temperature for 3h, acetone (2 mL) was added to the reaction and the mixture was stirred at room temperature for 18h. The reaction mixture was diluted with ethyl acetate and washed with water and brine. The organic layer was dried over magnesium sulfate, concentrated and purified by flash column chromatography (25 g, 0–60% ethyl acetate/hexanes) to obtain 75 mg of 4-bromo-N-(3,5-dibromophenyl)-3-oxobutanamide as a pink solid. To this was added sulfuric acid (0.100 mL, 1.8 mmol) and the mixture stirred at 45 °C for 18h. Cold water was then added to the reaction mixture and the resulting precipitate filtered, washed with dichloromethane, and dried to obtain 65 mg (61%) of 5,7-dibromo-4-(bromomethyl)-1,2-dihydroquinolin-2-one as a beige solid that was used in the next step without further purification. ¹H NMR (400 MHz, *d*₆-DMSO) δ 12.15 (br.s, 1H), 7.75 (s, 1H), 7.56 (s, 1H), 6.92 (s, 1H), 5.19 (s, 2H). ¹³C NMR (100 MHz, *d*₆-DMSO) δ 160.56, 146.96, 143.17, 131.48, 127.39, 123.76, 120.11, 119.14, 115.43, 33.99. Step 3. A mixture of 5,7-dibromo-4-(bromomethyl)-1,2-dihydroquinolin-2-one (0.055 g, 0.14 mmol) and triethyl phosphite (0.24 mL, 1.4 mmol) was stirred in dioxane (3.0 mL) at 100 °C for 24 h. The reaction mixture was concentrated and the residue purified by flash column chromatography (0–10% methanol/dichloromethane) to obtain 62 mg (98%) of diethyl [(5,7-dibromo-2-oxo-1,2-dihydroquinolin-4-yl)methyl]phosphonate as a beige solid. ¹H NMR (400 MHz, CDCl₃) δ 12.83 (br.s, 1H), 7.57–7.66 (m, 2H), 6.77 (d, *J* = 4.6 Hz, 1H), 4.08–4.41 (m, 6H), 1.29 (t, *J* = 7.1 Hz, 6H). ¹³C NMR (100 MHz, CDCl₃) δ 162.22, 143.96, 143.86, 141.71, 132.89, 126.12, 124.11, 120.06, 119.74, 117.11, 62.76, 62.60, 34.16, 32.80, 16.43, 16.37. LC-MS: *m/z* = 453 [M+H]⁺. Step 4. A mixture of diethyl [(5,7-dibromo-2-oxo-1,2-dihydroquinolin-4-yl)methyl]phosphonate (0.035 g, 0.077 mmol) and 4 M solution of hydrochloric acid in dioxane (1.0 mL) was stirred at 100 °C for 24 h. The reaction mixture was then concentrated to dryness and purified by reverse phase HPLC to obtain 18 mg (58%) of the product (**16**) as a white solid. ¹H NMR (400 MHz, *d*₆-DMSO) δ 7.65 (d, *J* = 1.8 Hz, 1H), 7.52 (d, *J* = 1.8 Hz, 1H), 6.57 (d, *J* = 4.1 Hz, 1H), 3.73 – 3.97 (m, 2H). LC-MS: *m/z* = 397 [M+H]⁺

Cloning of the KPC-2, NDM-1, and VIM-2 genes.—For KPC-2, the gene encoding residues 25–293 was cloned into the pET-GST vector as an N-terminal 6X His-tag protein. For NDM-1, two constructs were used. NDM-1 construct 1 encoding residues 29–270 inserted into the pET-SUMO vector with an N-terminal 6X His/SUMO tag was a kind gift from Dr. Hongmin Zhang and Dr. Quan Hao. NDM-1 construct 1 was used for enzymatic assays. NDM-1 construct 2 encoding residues 42–270 was cloned using standard restriction enzyme cloning techniques into a pET28a vector with an N-terminal 6X His-tag and a

thrombin cleavage site. NDM-1 construct 2 was used for crystallization. The gene encoding VIM-2 was custom synthesized (ATUM/DNA2.0) and inserted into the vector pD441-SR with an N-terminal 6X His-tag and a TEV cleavage site. NDM-1 constructs were transformed into NEB 5-alpha competent *E. coli* and plated on LB agar containing either 100 µg/mL ampicillin (NDM-1 construct 1) or 50 µg/mL kanamycin (NDM-1 construct 2). Single colonies of the NDM-1 constructs were grown overnight at 30 °C in LB media containing either 100 µg/mL ampicillin or 50 µg/mL kanamycin. Cells were collected, and the plasmid DNA was isolated using a mini-prep kit. The nucleotide sequence of both NDM-1 constructs were verified. The D199N mutation was performed in NDM-1 by site-directed mutagenesis using QuikChange and its sequence verified.

Protein expression and purification.—KPC-2 was expressed and purified as previously described^{4, 67}. Recombinant NDM-1 and VIM-2 were produced in either *E. coli* BL21(DE3) cells (NDM-1 constructs) or Rosetta 2 (DE3) cells (VIM-2) and grown at 37 °C using Terrific broth supplemented with either 100 µg/mL ampicillin (NDM-1 construct 1), 50 µg/mL kanamycin (NDM-1 construct 2), or 50 µg/mL kanamycin + 35 µg/mL chloramphenicol (VIM-2) until the OD₆₀₀ reached 0.8–1.0. Expression of NDM-1 and VIM-2 were initiated by the addition of 0.5 mM IPTG and 0.1 mM zinc sulfate and the cultures were incubated at 20 °C for an additional 22 h. Cells were collected by centrifugation (6,000g/20 min, 4 °C) then resuspended and sonicated in either 20 mM HEPES pH 7.4, 500 mM NaCl, 20 mM imidazole for the NDM-1 constructs or 50 mM HEPES pH 7.5, 150 mM NaCl, 20 mM imidazole, 50 mM zinc sulfate for VIM-2. One complete EDTA-free protease inhibitor tablet was added before sonication. The lysate was centrifuged (45,000 rpm/1 h, 4 °C), filtered, and the soluble proteins were separated by nickel affinity chromatography using a HisTrap HP (GE Healthcare) column, and the proteins were eluted over a 500 mM imidazole gradient. Briefly, NDM-1 construct 1 was purified as followed. The fractions containing protein from the nickel affinity chromatography were pooled and dialyzed against 20 mM HEPES pH 7.0, 100 mM NaCl. Cleavage of the N-terminal 6X His/SUMO was carried out using ULP1 overnight at 20 °C. The affinity tag was removed by loading the sample onto a HisTrap HP column pre-equilibrated with 20 mM HEPES pH 7.0, 100 mM NaCl and collecting the flow through, which contained the cleaved protein. The sample was concentrated and loaded onto a HiLoad 16/600 Superdex 75 pg (GE Healthcare) pre-equilibrated with 20 mM HEPES pH 7.0, 100 mM NaCl. The protein concentration was measured spectrophotometrically using the predicted extinction coefficient ($\epsilon_{280} = 27,960 \text{ cm}^{-1} \text{ M}^{-1}$). NDM-1 construct 2 was purified in an identical manner as NDM-1 construct 1, except that the N-terminal 6X His-tag was removed using thrombin overnight at 4 °C overnight. Briefly, VIM-2 was purified as followed. The fractions containing protein from the nickel affinity chromatography were pooled and dialyzed into 50 mM Tris-HCl pH 8.0, 150 mM NaCl, 1 mM DTT. Cleavage of the N-terminal 6X His-tag was carried out using the TEV protease overnight at 25 °C. The affinity tag was removed by loading the sample onto a HisTrap HP column pre-equilibrated with 50 mM Tris-HCl pH 8.0, 150 mM NaCl, 1 mM DTT and collecting the flow through, which contained the cleaved protein. The sample was concentrated and loaded onto a HiLoad 16/600 Superdex 75 pg (GE Healthcare) pre-equilibrated with 50 mM HEPES pH 7.5, 150 mM NaCl, 50 mM zinc sulfate. The protein concentration was measured

spectrophotometrically using the predicted extinction coefficient ($\epsilon_{280} = 29,910 \text{ cm}^{-1} \text{ M}^{-1}$).

Enzyme kinetics.—All kinetic data were determined in duplicate using a Biotek Cytation Multi-Mode Reader at 37 °C. For KPC-2, assays were performed in 100 mM Tris-HCl pH 7.0, 0.01% (v/v) Triton X-100 and 1 nM KPC-2 enzyme. For NDM-1 (construct 1) and VIM-2, the assays were performed in 50 mM HEPES pH 7.2, 50 μM zinc sulfate, 0.01% (v/v) Triton X-100, 20 $\mu\text{g/mL}$ BSA. NDM-1 enzyme concentration was 2 nM and VIM-2 enzyme concentration was 0.5 nM. All the reactions were initiated by the addition of enzyme and the reaction progress curves were followed spectrophotometrically. Initial steady-state velocities from nitrocefin hydrolysis was measured at a wavelength of 486 nm. Using SigmaPlot 12.5, the V_{max} and K_{m} of nitrocefin were determined by non-linear regression using the Michaelis-Menten equation. β -Lactamase activity was measured in the presence of increasing amount of the inhibitors. The IC_{50} was obtained from the sigmoidal concentration dependence curve calculated using SigmaPlot 12.5. The K_i of each inhibitor was calculated according to the Cheng-Prusoff equation⁷¹: $K_i = \text{IC}_{50} / (1 + [S]/K_m)$, where [S] is the nitrocefin concentration, K_m is the Michaelis constant of the enzymes. All assays were performed in duplicate except compound **1** (tested once due to compound availability) and compound **16** (triplicate).

Computational docking.—The program DOCK 3.5.4^{72, 73} was used to screen the fragment subset of the ZINC database²⁸ of small molecules, a free database containing a large number of commercially available compounds and frequently used by both academic and industry researchers. The virtual screening experiment was carried out using a deposited KPC-2 structure (PDB ID 5UL8) as receptor template and a previously described procedure³⁵. Briefly, all water molecules were removed from the protein except for the catalytic water and water molecule in the oxyanion hole. Hydrogen atoms were added by the docking program and energy potential grids were calculated. The partial charges of those polar active site residues known to interact with substrates (e.g. S70, N132) were increased to favor such interactions with the ligand. The top 1000 compounds were visually examined to select compounds to purchase.

Crystallization.—KPC-2 was crystallized and soaked as described previously⁶⁷. NDM-1 construct 2 (residues 42–270) was used to generate crystals. NDM-1 crystals were grown at 20 °C using the hanging-drop vapor diffusion method. Protein solutions (10–20 mg/mL) in 20 mM HEPES pH 7.0, 100 mM NaCl were mixed 1:1 (v/v) with reservoir solution containing 50 mM potassium phosphate monobasic, 10 mM calcium chloride, and 25% (w/v) PEG 8,000. Crystals typically formed in 2 days. To obtain the ligand bound structures, NDM-1 crystals were soaked in a solution of 50 mM sodium acetate pH 3.85, 25% (w/v) PEG 8,000 and 10 mM inhibitor for 1 h. The soaked crystals were cryo-protected in a solution containing 50 mM sodium acetate pH 3.85, 25% (w/v) PEG 8,000, and 20% (v/v) glycerol and flash-cooled in liquid nitrogen. For NDM-1 D199N mutant, a 15 mg/mL protein stock was used to grow crystals in 0.05 M potassium phosphate dibasic (pH-8.0), 0.01 M calcium chloride, 25% (w/v) PEG8000. Complex NDM-1 D199N mutant crystals were prepared via soaking in 0.05 M sodium acetate pH 7.5, 20% (w/v) PEG 8,000 and 10

mM inhibitors for about 1–2 hour. The soaked crystals were cryo-protected in a solution the same as the soaking conditions but with added 20% (v/v) glycerol, and flash-cooled in liquid nitrogen. Crystals of VIM-2 were grown at 20 °C using hanging-drop vapor diffusion. Protein solutions (10–20 mg/mL) in 50 mM HEPES pH 7.0, 150 mM NaCl, and 50 μ M zinc sulfate were mixed 1:1 (v/v) with reservoir solution containing 200 mM calcium acetate (pH 7.0), 20% (w/v) PEG 3,350, and 1 mM TCEP. Crystals typically formed in 2 days. To obtain the ligand bound structures at low pH, VIM-2 crystals were soaked in a solution of 50 mM sodium acetate pH 3.85, 25% (w/v) PEG 8,000 and 10 mM inhibitor for 1 hour. The soaked crystals were cryo-protected in a solution containing 50 mM sodium acetate pH 3.85, 25% (w/v) PEG 8,000, and 20% (v/v) glycerol and flash-cooled in liquid nitrogen. For higher pH complex structures, VIM-2 complex crystals were prepared via soaking in 0.05 M sodium acetate pH 7.5, 20% (w/v) PEG8000 and 10 mM inhibitors for about 1 hour. The soaked crystals were cryo-protected in a solution the same as the soaking conditions but with added 20% (v/v) glycerol, and flash-cooled in liquid nitrogen.

Data collection and structure determinations.—Data for the KPC-2, NDM-1, and VIM-2 complex structures were collected using beamlines 19-BM-D, 22-BM-D, and 22-ID-D at the Advanced Photon Source (APS), Argonne National Laboratory (ANL) and beamline 8.3.1 at the Advanced Light Source (ALS), Lawrence Berkeley National Laboratory (LBNL). Diffraction data were indexed and integrated with iMosflm⁷⁴ and scaled with SCALA⁷⁵ from the CCP4 suite⁷⁶. Phasing was performed using molecular replacement with the program Phaser⁷⁷ of the PHENIX suite⁷⁸, with the KPC-2 structure (PDB ID 5UL8), NDM-8 (PDB ID 4TZF), and VIM-2 (PDB ID 1KO3). Structure refinement was performed using phenix.refine⁷⁹ of the PHENIX suite and model building in WinCoot⁸⁰. The composite simulated annealing mF_o-DF_c omit maps were generated using the composite omit map program⁸¹ from the PHENIX suite. The program eLBOW of the PHENIX suite was used to obtain geometry restraint information⁸². The final model qualities were assessed using MolProbity⁸³. Statistics for data collection and refinement are given in Supporting Information Table 1. All protein structure figures were generated using PyMOL 2.3.2 (Schrödinger).

Susceptibility testing.—Microbiological testing of compounds **9**, **11**, and **13** was performed under contract with Micromyx, LLC (Kalamazoo, MI). Test medium used was Mueller Hinton II broth (MHBII; Lot No.5257869; Becton Dickinson, Sparks, MD). The media was prepared and stored according to guidelines from the Clinical and Laboratory Standards Institute (CLSI)⁸⁴. The test isolates consisted of Gram-negative pathogens from the Micromyx repository. Relevant quality control organisms from the American Type Culture Collection (ATCC) were included as directed by CLSI guidelines. The MIC assay method followed the procedure described by CLSI and employed automated liquid handlers to conduct serial dilutions and liquid transfers. Automated liquid handlers included the Multidrop 384 (Labsystems, Helsinki, Finland), Biomek 2000 and Biomek FX. The Biomek 2000 was used to perform serial two-fold dilutions of test compound. A standardized inoculum of each organism was prepared per CLSI methods. Colonies were picked from the primary plate and a suspension was prepared to equal a 0.5 McFarland turbidity standard. Suspensions were diluted 1:20 in MHBII medium and then transferred to compartments of

sterile reservoirs divided by length (Beckman Coulter). The Biomek 2000 was used to inoculate the plates. Daughter plates were placed on the Biomek 2000 in reverse orientation so that plates were inoculated from low to high drug concentration. The Biomek 2000 delivered 10 μL of standardized inoculum into each well of the appropriate daughter plate for an additional 1:20 dilution, resulting in a final concentration of approximately 5×10^5 CFU per well. Thus, the wells of the daughter plates ultimately contained 185 μL of MHBII, 5 μL of drug solution, and 10 μL of inoculum. Plates were stacked 3 high, covered with a lid on the top plate, placed into plastic bags, and incubated at 35 °C for 18–20 h. Plates were viewed from the bottom using a plate viewer. An un-inoculated solubility control plate was observed for evidence of drug precipitation. MICs were read where visible growth of the organism was inhibited. Compounds **9**, **11**, and **13** were tested alone in the concentration range 128 – 0.12 $\mu\text{g}/\text{mL}$ and returned MIC > 128 $\mu\text{g}/\text{mL}$ against all strains. Compounds **9**, **11**, and **13** were tested at a fixed concentration of 128 $\mu\text{g}/\text{mL}$ in combination with imipenem in a concentration range of 128 – 0.001 $\mu\text{g}/\text{mL}$. The positive control was avibactam (4 $\mu\text{g}/\text{mL}$) in combination with ceftazidime in the range 64 – 0.006 $\mu\text{g}/\text{mL}$.

Checkerboard assays.—The isogenic *P. aeruginosa* strains expressing various carbapenemases were a kind gift from Dr. Olga Lomovskaya of QPex Biopharma Inc. A strain lacking efflux pumps was constructed using the parent strain PAM1154 and by disrupting the *oprM* gene to inactivate two major efflux pumps that are constitutively expressed, MexAB-OprM and MexYX-OprM. The strain overexpressing efflux pumps was constructed using the parent strain PAM1032 with a mutation in the negative regulator *mexR* to overexpress MexAB-OprM. Plasmids carrying various carbapenemase genes, including vector only controls, were then transformed into these two strains.

The clinical *K. pneumoniae* strain was kindly provided by Dr. Yohei Doi (University of Pittsburgh). The MIC of imipenem against all strains was determined prior to combining treatments according to CLSI guidelines. Bacterial cultures were stored in glycerol stocks at –80°C and were streaked onto Luria-Broth supplemented with (15 $\mu\text{g}/\text{mL}$ gentamicin for QPex strains) or without antibiotic. Stock plates were grown for 18 h at 37°C prior to storage at 4°C for no longer than 3 days. Prior to each assay, single colonies were resuspended in tryptic soy broth (TSB) supplemented with or without antibiotic and were incubated for approximately 20 h shaking at 37°C. MHBII was used for all assays in a 96 well plate format. For each assay, the inhibitor was tested at a concentration of 128 $\mu\text{g}/\text{mL}$ – 2 $\mu\text{g}/\text{mL}$ decreasing two-fold across each row. Imipenem was tested starting at the MIC and decreasing two-fold across each column. Avibactam was tested in combination with imipenem at a concentration of 16 $\mu\text{g}/\text{mL}$ –0.25 $\mu\text{g}/\text{mL}$ across each row with imipenem tested at 512 $\mu\text{g}/\text{mL}$ – 0.5 $\mu\text{g}/\text{mL}$ across each column. The plates were incubated shaking at 37°C for approximately 20 h and were then quantified by reading the optical density (OD₆₀₀) using a synergy 2 plate reader (BioTek). Inhibition was defined in wells exhibiting an optical density equal to media only wells.

Cytotoxicity testing.—To assess the toxicity of the compounds, Hek293T human embryonic kidney epithelial cells were used. Viability was determined using 3-(4,5-dimethylthiazol-2-yl)-2,5-diphenyltetrazolium bromide (MTT) as a molecular probe. The

assay was carried out as previously described by our group⁸⁵. In brief, compounds dissolved in dimethyl-sulfoxide (DMSO) were tested at a range of 200 µg/mL-3.125 µg/mL utilizing two-fold dilutions. Cells were grown in DMEM supplemented with 10% FBS and 1% penicillin/streptomycin. Cells were treated for 48 hours and incubated at 37°C in 5% CO₂. Following treatment, MTT was added and measured at an OD of 570nm using a Biotek Synergy 2 plate reader. Percent recovery was then calculated compared to solvent only controls.

ADME analysis.—Microsome stability and MDCK-MDR permeability studies were performed at Quintara Biosciences (South San Francisco, CA). Kinetic solubility studies were performed at Analiza (Cleveland, OH).

Supplementary Material

Refer to Web version on PubMed Central for supplementary material.

Acknowledgement

The authors acknowledge financial support from the National Institutes of Health (NIH) grant AI103158 (Y.C.) and AI124458 (L.N.S.) and from the National Center for Advancing Translational Science UCSF-CTSI Grant UL1 TR000004 (A.R.R.). We thank Dr. Hongmin Zhang and Dr. Quan Hao (University of Hong Kong) for the NDM-1 clone, Dr. Olga Lomovskaya (QPex Biopharma Inc.) for the *P. aeruginosa* isogenic strains, and Dr. Yohei Doi (University of Pittsburgh) for the *K. pneumoniae* clinical strain. We thank the staffs of beamlines 19-BM, 22-BM, and 22-ID at APS and the staffs of beamline 8.3.1 at ALS.

Abbreviations Used

SBL	serine β-lactamase
MBL	metallo-β-lactamase
KPC-2	<i>Klebsiella pneumoniae</i> carbapenemase-2
NDM-1	New Delhi metallo-β-lactamase-1
VIM-2	Verona integron-encoded metallo-β-lactamase-2
OXA-48	oxacillinase-48
CRE	carbapenem-resistant <i>Enterobacteriaceae</i>
FBLD	fragment-based lead discovery
SAR	structure-activity relationship
NMR	nuclear magnetic resonance
LC-MS	liquid chromatography–mass spectrometry
L.E.	ligand efficiency
HB	hydrogen bond
MIC	minimum inhibitory concentration

ADME	absorption, distribution, metabolism and excretion
DHQ	dihydroquinolinone
DMSO	dimethyl sulfoxide
TCEP	tris(2-carboxyethyl)phosphine
IPTG	isopropyl β -D-1-thiogalactopyranoside
PEG	polyethylene glycol
EDTA	ethylenediaminetetraacetic acid
DTT	dithiothreitol
HCl	hydrochloric acid
PDB	Protein Data Bank
WT	wild type
HEK	human embryonic kidney
PBS	phosphate buffered saline
TEV	tobacco etch virus
SUMO	small ubiquitin-like modifier
BSA	bovine serum albumin

References

1. Cho H; Uehara T; Bernhardt TG β -lactam antibiotics induce a lethal malfunctioning of the bacterial cell wall synthesis machinery. *Cell* 2014, 159, 1300–1311. [PubMed: 25480295]
2. Bush K; Fisher JF Epidemiological expansion, structural studies, and clinical challenges of new β -lactamases from gram-negative bacteria. *Annu Rev Microbiol* 2011, 65, 455–478. [PubMed: 21740228]
3. Bush K; Jacoby GA Updated functional classification of β -lactamases. *Antimicrob Agents Chemother* 2010, 54, 969–976. [PubMed: 19995920]
4. Palzkill T Metallo- β -lactamase structure and function. *Ann N Y Acad Sci* 2013, 1277, 91–104. [PubMed: 23163348]
5. Nordmann P; Dortet L; Poirel L Carbapenem resistance in Enterobacteriaceae: here is the storm! *Trends Mol Med* 2012, 18, 263–272. [PubMed: 22480775]
6. Trecarichi EM; Tumbarello M Therapeutic options for carbapenem-resistant Enterobacteriaceae infections. *Virulence* 2017, 8, 470–484. [PubMed: 28276996]
7. Papp-Wallace KM; Endimiani A; Taracila MA; Bonomo RA Carbapenems: past, present, and future. *Antimicrob Agents Chemother* 2011, 55, 4943–4960. [PubMed: 21859938]
8. van Duin D; Kaye KS; Neuner EA; Bonomo RA Carbapenem-resistant *Enterobacteriaceae*: a review of treatment and outcomes. *Diagn Microbiol Infect Dis* 2013, 75, 115–120. [PubMed: 23290507]
9. Morrill HJ; Pogue JM; Kaye KS; LaPlante KL Treatment options for carbapenem-resistant Enterobacteriaceae infections. *Open Forum Infect Dis* 2015, 2, ofv050. [PubMed: 26125030]

10. Aloush V; Navon-Venezia S; Seigman-Igra Y; Cabili S; Carmeli Y Multidrug-resistant *Pseudomonas aeruginosa*: risk factors and clinical impact. *Antimicrob Agents Chemother* 2006, 50, 43–48. [PubMed: 16377665]
11. Lutgring JD; Limbago BM The problem of carbapenemase-producing-carbapenem-resistant-*Enterobacteriaceae* detection. *J Clin Microbiol* 2016, 54, 529–534. [PubMed: 26739152]
12. Meletis G Carbapenem resistance: overview of the problem and future perspectives. *Ther Adv Infect Dis* 2016, 3, 15–21. [PubMed: 26862399]
13. Ho PL; Cheung YY; Wang Y; Lo WU; Lai EL; Chow KH; Cheng VC Characterization of carbapenem-resistant *Escherichia coli* and *Klebsiella pneumoniae* from a healthcare region in Hong Kong. *Eur J Clin Microbiol Infect Dis* 2016, 35, 379–385. [PubMed: 26740321]
14. Queenan AM; Bush K Carbapenemases: the versatile β -lactamases. *Clin Microbiol Rev* 2007, 20, 440–458. [PubMed: 17630334]
15. Walsh TR; Toleman MA; Poirel L; Nordmann P Metallo- β -lactamases: the quiet before the storm? *Clin Microbiol Rev* 2005, 18, 306–325. [PubMed: 15831827]
16. Papp-Wallace KM; Bonomo RA New β -lactamase inhibitors in the clinic. *Infect Dis Clin North Am* 2016, 30, 441–464. [PubMed: 27208767]
17. Sun Z; Hu L; Sankaran B; Prasad BVV; Palzkill T Differential active site requirements for NDM-1 β -lactamase hydrolysis of carbapenem versus penicillin and cephalosporin antibiotics. *Nature communications* 2018, 9, 4524.
18. King AM; Reid-Yu SA; Wang W; King DT; De Pascale G; Strynadka NC; Walsh TR; Coombes BK; Wright GD Aspergillomarasmine A overcomes metallo- β -lactamase antibiotic resistance. *Nature* 2014, 510, 503–506. [PubMed: 24965651]
19. Watkins RR; Papp-Wallace KM; Drawz SM; Bonomo RA Novel β -lactamase inhibitors: a therapeutic hope against the scourge of multidrug resistance. *Front Microbiol* 2013, 4, 392. [PubMed: 24399995]
20. Ehmann DE; Jahic H; Ross PL; Gu RF; Hu J; Kern G; Walkup GK; Fisher SL Avibactam is a covalent, reversible, non- β -lactam β -lactamase inhibitor. *Proc Natl Acad Sci U S A* 2012, 109, 11663–11668. [PubMed: 22753474]
21. Abboud MI; Dambon C; Brem J; Smargiasso N; Mercuri P; Gilbert B; Rydzik AM; Claridge TD; Schofield CJ; Frere JM Interaction of avibactam with class B metallo- β -lactamases. *Antimicrob Agents Chemother* 2016, 60, 5655–5662. [PubMed: 27401561]
22. Castanheira M; Rhomberg PR; Flamm RK; Jones RN Effect of the β -lactamase inhibitor vaborbactam combined with meropenem against serine carbapenemase-producing *Enterobacteriaceae*. *Antimicrob Agents Chemother* 2016, 60, 5454–5458. [PubMed: 27381386]
23. Brem J; Cain R; Cahill S; McDonough MA; Clifton IJ; Jimenez-Castellanos JC; Avison MB; Spencer J; Fishwick CW; Schofield CJ Structural basis of metallo- β -lactamase, serine- β -lactamase and penicillin-binding protein inhibition by cyclic boronates. *Nature communications* 2016, 7, 12406.
24. Cahill ST; Cain R; Wang DY; Lohans CT; Wareham DW; Oswin HP; Mohammed J; Spencer J; Fishwick CW; McDonough MA; Schofield CJ; Brem J Cyclic boronates inhibit all classes of β -lactamases. *Antimicrob Agents Chemother* 2017, 61, e02260–16. [PubMed: 28115348]
25. Brown ED; Wright GD Antibacterial drug discovery in the resistance era. *Nature* 2016, 529, 336–343. [PubMed: 26791724]
26. Reynolds CH Ligand efficiency metrics: why all the fuss? *Future Med Chem* 2015, 7, 1363–1365. [PubMed: 26230875]
27. Li GB; Abboud MI; Brem J; Someya H; Lohans CT; Yang SY; Spencer J; Wareham DW; McDonough MA; Schofield CJ NMR-filtered virtual screening leads to non-metal chelating metallo- β -lactamase inhibitors. *Chem Sci* 2017, 8, 928–937. [PubMed: 28451231]
28. Irwin JJ; Shoichet BK ZINC--a free database of commercially available compounds for virtual screening. *J Chem Inf Model* 2005, 45, 177–182. [PubMed: 15667143]
29. Huggins DJ; Sherman W; Tidor B Rational approaches to improving selectivity in drug design. *J Med Chem* 2012, 55, 1424–1444. [PubMed: 22239221]
30. Zhang H; Hao Q Crystal structure of NDM-1 reveals a common β -lactam hydrolysis mechanism. *FASEB J* 2011, 25, 2574–2582. [PubMed: 21507902]

31. Feng H; Ding J; Zhu D; Liu X; Xu X; Zhang Y; Zang S; Wang DC; Liu W Structural and mechanistic insights into NDM-1 catalyzed hydrolysis of cephalosporins. *Journal of the American Chemical Society* 2014, 136, 14694–14697. [PubMed: 25268575]
32. Brown MC; Verma D; Russell C; Jacobs DJ; Livesay DR A case study comparing quantitative stability-flexibility relationships across five metallo- β -lactamases highlighting differences within NDM-1. *Methods Mol Biol* 2014, 1084, 227–238. [PubMed: 24061924]
33. Papp-Wallace KM; Taracila M; Wallace CJ; Hujer KM; Bethel CR; Hornick JM; Bonomo RA Elucidating the role of Trp105 in the KPC-2 β -lactamase. *Protein Sci* 2010, 19, 1714–1727. [PubMed: 20662006]
34. Hamilton GSB, D.; Borosky, S.A.; Huang, Z.; Zubrowski, R.; Ferkany, J.W.; Karbon, E.W. Synthesis and glutamate antagonist activity of 4-phosphonoalkylquinoline derivatives: a novel class of non-NMDA antagonist. *Bioorg. Med. Chem. Lett* 1994, 4, 2035–2040.
35. Chen Y; Shoichet BK Molecular docking and ligand specificity in fragment-based inhibitor discovery. *Nature chemical biology* 2009, 5, 358–364. [PubMed: 19305397]
36. Teotico DG; Babaoglu K; Rocklin GJ; Ferreira RS; Giannetti AM; Shoichet BK Docking for fragment inhibitors of AmpC β -lactamase. *Proc Natl Acad Sci U S A* 2009, 106, 7455–7460. [PubMed: 19416920]
37. Rahil J; Pratt RF Phosphonate monoester inhibitors of class A β -lactamases. *Biochem J* 1991, 275, 793–795. [PubMed: 1903928]
38. Lobkovsky E; Billings EM; Moews PC; Rahil J; Pratt RF; Knox JR Crystallographic structure of a phosphonate derivative of the *Enterobacter cloacae* P99 cephalosporinase: mechanistic interpretation of a β -lactamase transition-state analog. *Biochemistry* 1994, 33, 6762–6772. [PubMed: 8204611]
39. Kumar S; Adediran SA; Nukaga M; Pratt RF Kinetics of turnover of cefotaxime by the *Enterobacter cloacae* P99 and GCI β -lactamases: two free enzyme forms of the P99 β -lactamase detected by a combination of pre- and post-steady state kinetics. *Biochemistry* 2004, 43, 2664–2672. [PubMed: 14992604]
40. Silvaggi NR; Kaur K; Adediran SA; Pratt RF; Kelly JA Toward better antibiotics: crystallographic studies of a novel class of DD-peptidase/ β -lactamase inhibitors. *Biochemistry* 2004, 43, 7046–7053. [PubMed: 15170342]
41. Lassaux P; Hamel M; Gulea M; Delbruck H; Mercuri PS; Horsfall L; Dehareng D; Kupper M; Frere JM; Hoffmann K; Galleni M; Bebrone C Mercaptophosphonate compounds as broad-spectrum inhibitors of the metallo- β -lactamases. *J Med Chem* 2010, 53, 4862–4876. [PubMed: 20527888]
42. Skagseth S; Akhter S; Paulsen MH; Muhammad Z; Lauksund S; Samuelsen O; Leiros HS; Bayer A Metallo- β -lactamase inhibitors by bioisosteric replacement: preparation, activity and binding. *European journal of medicinal chemistry* 2017, 135, 159–173. [PubMed: 28445786]
43. Hinchliffe P; Tanner CA; Krismanich AP; Labbe G; Goodfellow VJ; Marrone L; Desoky AY; Calvopina K; Whittle EE; Zeng F; Avison MB; Bols NC; Siemann S; Spencer J; Dmitrienko GI Structural and kinetic studies of the potent inhibition of metallo- β -lactamases by 6-Phosphonomethylpyridine-2-carboxylates. *Biochemistry* 2018, 57, 1880–1892. [PubMed: 29485857]
44. Zhang C; Pu Y.-c.; Yu Z.-J; Wu C.-y.; Brem J; McDonough MA; Schofield CJ; Li G.-B; Wu Y. Rh(iii)-catalyzed directed C–H carbenoid coupling reveals aromatic bisphosphonates inhibiting metallo and serine- β -lactamases. *Organic Chemistry Frontiers* 2018, 5, 1288–1292.
45. Hinchliffe P; Gonzalez MM; Mojica MF; Gonzalez JM; Castillo V; Saiz C; Kosmopoulou M; Tooke CL; Llarrull LI; Mahler G; Bonomo RA; Vila AJ; Spencer J Cross-class metallo- β -lactamase inhibition by bisthiazolidines reveals multiple binding modes. *Proc Natl Acad Sci U S A* 2016, 113, E3745–E3754. [PubMed: 27303030]
46. Gonzalez MM; Kosmopoulou M; Mojica MF; Castillo V; Hinchliffe P; Pettinati I; Brem J; Schofield CJ; Mahler G; Bonomo RA; Llarrull LI; Spencer J; Vila AJ Bisthiazolidines: a substrate-mimicking scaffold as an inhibitor of the NDM-1 carbapenemase. *ACS infectious diseases* 2015, 1, 544–554. [PubMed: 27623409]

47. Papp-Wallace KM; Nguyen NQ; Jacobs MR; Bethel CR; Barnes MD; Kumar V; Bajaksouzian S; Rudin SD; Rather PN; Bhavsar S; Ravikumar T; Deshpande PK; Patil V; Yeole R; Bhagwat SS; Patel MV; van den Akker F; Bonomo RA Strategic approaches to overcome resistance against gram-negative pathogens using β -lactamase inhibitors and β -lactam enhancers: activity of three novel diazabicyclooctanes WCK 5153, zidebactam (WCK 5107), and WCK 4234. *J Med Chem* 2018, 61, 4067–4086. [PubMed: 29627985]
48. Akhter S; Lund BA; Ismael A; Langer M; Isaksson J; Christopeit T; Leiros HS; Bayer A A focused fragment library targeting the antibiotic resistance enzyme oxacillinase-48: synthesis, structural evaluation and inhibitor design. *European journal of medicinal chemistry* 2018, 145, 634–648. [PubMed: 29348071]
49. Caselli E; Romagnoli C; Powers RA; Taracila MA; Bouza AA; Swanson HC; Smolen KA; Fini F; Wallar BJ; Bonomo RA; Prati F Inhibition of Acinetobacter-derived cephalosporinase: exploring the carboxylate recognition site using novel β -lactamase inhibitors. *ACS infectious diseases* 2018, 4, 337–348. [PubMed: 29144725]
50. Bouza AA; Swanson HC; Smolen KA; VanDine AL; Taracila MA; Romagnoli C; Caselli E; Prati F; Bonomo RA; Powers RA; Wallar BJ Structure-based analysis of boronic acids as inhibitors of Acinetobacter-derived cephalosporinase-7, a unique class C β -lactamase. *ACS infectious diseases* 2018, 4, 325–336. [PubMed: 29144724]
51. Werner JP; Mitchell JM; Taracila MA; Bonomo RA; Powers RA Exploring the potential of boronic acids as inhibitors of OXA-24/40 β -lactamase. *Protein Sci* 2017, 26, 515–526. [PubMed: 27997706]
52. Nguyen NQ; Krishnan NP; Rojas LJ; Prati F; Caselli E; Romagnoli C; Bonomo RA; van den Akker F Crystal structures of KPC-2 and SHV-1 β -lactamases in complex with the boronic acid transition state analog S02030. *Antimicrob Agents Chemother* 2016, 60, 1760–1766. [PubMed: 26729491]
53. Rojas LJ; Taracila MA; Papp-Wallace KM; Bethel CR; Caselli E; Romagnoli C; Winkler ML; Spellberg B; Prati F; Bonomo RA Boronic acid transition state inhibitors active against KPC and other class A β -lactamases: structure-activity relationships as a guide to inhibitor design. *Antimicrob Agents Chemother* 2016, 60, 1751–1759. [PubMed: 26729496]
54. Spyarakis F; Bellio P; Quotadamo A; Linciano P; Benedetti P; D'Arrigo G; Baroni M; Cendron L; Celenza G; Tondi D First virtual screening and experimental validation of inhibitors targeting GES-5 carbapenemase. *Journal of computer-aided molecular design* 2019, 33, 295–305. [PubMed: 30603820]
55. Tilwawala R; Cammarata M; Adediran SA; Brodbelt JS; Pratt RF A new covalent inhibitor of class C β -lactamases reveals extended active site specificity. *Biochemistry* 2015, 54, 7375–7384. [PubMed: 26651220]
56. Nichols DA; Jaishankar P; Larson W; Smith E; Liu G; Beyrouthy R; Bonnet R; Renslo AR; Chen Y Structure-based design of potent and ligand-efficient inhibitors of CTX-M class A β -lactamase. *J Med Chem* 2012, 55, 2163–2172. [PubMed: 22296601]
57. Pembernton OA; Zhang X; Nichols DA; DeFrees K; Jaishankar P; Bonnet R; Adams J; Shaw LN; Renslo AR; Chen Y Antibacterial spectrum of a tetrazole-based reversible inhibitor of serine β -lactamases. *Antimicrob Agents Chemother* 2018, 62, e02563–17. [PubMed: 29844038]
58. Brem J; van Berkel SS; Aik W; Rydzik AM; Avison MB; Pettinati I; Umland KD; Kawamura A; Spencer J; Claridge TD; McDonough MA; Schofield CJ Rhodanine hydrolysis leads to potent thioenolate mediated metallo- β -lactamase inhibition. *Nature chemistry* 2014, 6, 1084–1090.
59. Chen P; Horton LB; Mikulski RL; Deng L; Sundriyal S; Palzkill T; Song Y 2-Substituted 4,5-dihydrothiazole-4-carboxylic acids are novel inhibitors of metallo- β -lactamases. *Bioorganic & medicinal chemistry letters* 2012, 22, 6229–6232. [PubMed: 22921080]
60. Cain R; Brem J; Zollman D; McDonough MA; Johnson RM; Spencer J; Makena A; Abboud MI; Cahill S; Lee SY; McHugh PJ; Schofield CJ; Fishwick CWG In silico fragment-based design identifies subfamily B1 metallo- β -lactamase inhibitors. *J Med Chem* 2018, 61, 1255–1260. [PubMed: 29271657]
61. Li GB; Brem J; Lesniak R; Abboud MI; Lohans CT; Clifton IJ; Yang SY; Jimenez-Castellanos JC; Avison MB; Spencer J; McDonough MA; Schofield CJ Crystallographic analyses of isoquinoline

- complexes reveal a new mode of metallo- β -lactamase inhibition. *Chemical communications* 2017, 53, 5806–5809. [PubMed: 28470248]
62. Linciano P; Cendron L; Gianquinto E; Spyarakis F; Tondi D Ten years with New Delhi Metallo- β -lactamase-1 (NDM-1): from structural insights to inhibitor design. *ACS infectious diseases* 2019, 5, 9–34. [PubMed: 30421910]
63. Santucci M; Spyarakis F; Cross S; Quotadamo A; Farina D; Tondi D; De Luca F; Docquier JD; Prieto AI; Ibacache C; Blazquez J; Venturelli A; Cruciani G; Costi MP Computational and biological profile of boronic acids for the detection of bacterial serine and metallo- β -lactamases. *Scientific reports* 2017, 7, 17716. [PubMed: 29255163]
64. Johnson JW; Gretes M; Goodfellow VJ; Marrone L; Heynen ML; Strynadka NC; Dmitrienko GI Cyclobutanone analogues of β -lactams revisited: insights into conformational requirements for inhibition of serine and metallo- β -lactamases. *Journal of the American Chemical Society* 2010, 132, 2558–2560. [PubMed: 20141132]
65. Devi P; Rutledge PJ Cyclobutanone analogues of β -lactam antibiotics: β -lactamase inhibitors with untapped potential? *Chembiochem : a European journal of chemical biology* 2017, 18, 338–351. [PubMed: 27992105]
66. Geibel B; Dowell J; Dickerson D; Henkel T 1401. A randomized, double-blind, placebo-controlled study of the safety and pharmacokinetics of single and repeat doses of VNRX-5133 in healthy subjects. *Open Forum Infectious Diseases* 2018, 5, S431.
67. Pemberton OA; Zhang X; Chen Y Molecular basis of substrate recognition and product release by the *Klebsiella pneumoniae* Carbapenemase (KPC-2). *J Med Chem* 2017, 60, 3525–3530. [PubMed: 28388065]
68. Bethel CR; Taracila M; Shyr T; Thomson JM; Distler AM; Hujer KM; Hujer AM; Endimiani A; Papp-Wallace K; Bonnet R; Bonomo RA Exploring the inhibition of CTX-M-9 by β -lactamase inhibitors and carbapenems. *Antimicrob Agents Chemother* 2011, 55, 3465–3475. [PubMed: 21555770]
69. Tomanicek SJ; Standaert RF; Weiss KL; Ostermann A; Schrader TE; Ng JD; Coates L Neutron and X-ray crystal structures of a perdeuterated enzyme inhibitor complex reveal the catalytic proton network of the Toho-1 β -lactamase for the acylation reaction. *J Biol Chem* 2013, 288, 4715–4722. [PubMed: 23255594]
70. Lahiri SD; Mangani S; Durand-Reville T; Benvenuti M; De Luca F; Sanyal G; Docquier JD Structural insight into potent broad-spectrum inhibition with reversible recyclization mechanism: avibactam in complex with CTX-M-15 and *Pseudomonas aeruginosa* AmpC β -lactamases. *Antimicrob Agents Chemother* 2013, 57, 2496–2505. [PubMed: 23439634]
71. Cheng Y; Prusoff WH Relationship between the inhibition constant (KI) and the concentration of inhibitor which causes 50 percent inhibition (I50) of an enzymatic reaction. *Biochem Pharmacol* 1973, 22, 3099–3108. [PubMed: 4202581]
72. Irwin JJ; Shoichet BK; Mysinger MM; Huang N; Colizzi F; Wassam P; Cao Y Automated docking screens: a feasibility study. *J Med Chem* 2009, 52, 5712–5720. [PubMed: 19719084]
73. Lorber DM; Udo MK; Shoichet BK Protein-protein docking with multiple residue conformations and residue substitutions. *Protein Sci* 2002, 11, 1393–1408. [PubMed: 12021438]
74. Battye TG; Kontogiannis L; Johnson O; Powell HR; Leslie AG iMOSFLM: a new graphical interface for diffraction-image processing with MOSFLM. *Acta Crystallogr D Biol Crystallogr* 2011, 67, 271–281. [PubMed: 21460445]
75. Evans P Scaling and assessment of data quality. *Acta Crystallogr D Biol Crystallogr* 2006, 62, 72–82. [PubMed: 16369096]
76. Winn MD; Ballard CC; Cowtan KD; Dodson EJ; Emsley P; Evans PR; Keegan RM; Krissinel EB; Leslie AG; McCoy A; McNicholas SJ; Murshudov GN; Pannu NS; Potterton EA; Powell HR; Read RJ; Vagin A; Wilson KS Overview of the CCP4 suite and current developments. *Acta Crystallogr D Biol Crystallogr* 2011, 67, 235–242. [PubMed: 21460441]
77. McCoy AJ; Grosse-Kunstleve RW; Adams PD; Winn MD; Storoni LC; Read RJ Phaser crystallographic software. *J Appl Crystallogr* 2007, 40, 658–674. [PubMed: 19461840]
78. Adams PD; Afonine PV; Bunkoczi G; Chen VB; Davis IW; Echols N; Headd JJ; Hung LW; Kapral GJ; Grosse-Kunstleve RW; McCoy AJ; Moriarty NW; Oeffner R; Read RJ; Richardson DC;

- Richardson JS; Terwilliger TC; Zwart PH PHENIX: a comprehensive python-based system for macromolecular structure solution. *Acta Crystallogr D Biol Crystallogr* 2010, 66, 213–221. [PubMed: 20124702]
79. Afonine PV; Grosse-Kunstleve RW; Echols N; Headd JJ; Moriarty NW; Mustyakimov M; Terwilliger TC; Urzhumtsev A; Zwart PH; Adams PD Towards automated crystallographic structure refinement with phenix.refine. *Acta Crystallogr D Biol Crystallogr* 2012, 68, 352–367. [PubMed: 22505256]
80. Emsley P; Lohkamp B; Scott WG; Cowtan K Features and development of Coot. *Acta Crystallogr D Biol Crystallogr* 2010, 66, 486–501. [PubMed: 20383002]
81. Terwilliger TC; Grosse-Kunstleve RW; Afonine PV; Moriarty NW; Adams PD; Read RJ; Zwart PH; Hung LW Iterative-build OMIT maps: map improvement by iterative model building and refinement without model bias. *Acta Crystallogr D Biol Crystallogr* 2008, 64, 515–524. [PubMed: 18453687]
82. Moriarty NW; Grosse-Kunstleve RW; Adams PD electronic Ligand Builder and Optimization Workbench (eLBOW): a tool for ligand coordinate and restraint generation. *Acta Crystallogr D Biol Crystallogr* 2009, 65, 1074–1080. [PubMed: 19770504]
83. Davis IW; Leaver-Fay A; Chen VB; Block JN; Kapral GJ; Wang X; Murray LW; Arendall WB 3rd; Snoeyink J; Richardson JS; Richardson DC MolProbity: all-atom contacts and structure validation for proteins and nucleic acids. *Nucleic Acids Res* 2007, 35, W375–383. [PubMed: 17452350]
84. Jorgensen JH; Ferraro MJ Antimicrobial susceptibility testing: a review of general principles and contemporary practices. *Clin Infect Dis* 2009, 49, 1749–1755. [PubMed: 19857164]
85. Fleeman RM; Debevec G; Antonen K; Adams JL; Santos RG; Welmaker GS; Houghten RA; Giulianotti MA; Shaw LN Identification of a novel polyamine scaffold with potent efflux pump inhibition activity toward multi-drug resistant bacterial pathogens. *Front Microbiol* 2018, 9, 1301. [PubMed: 29963035]

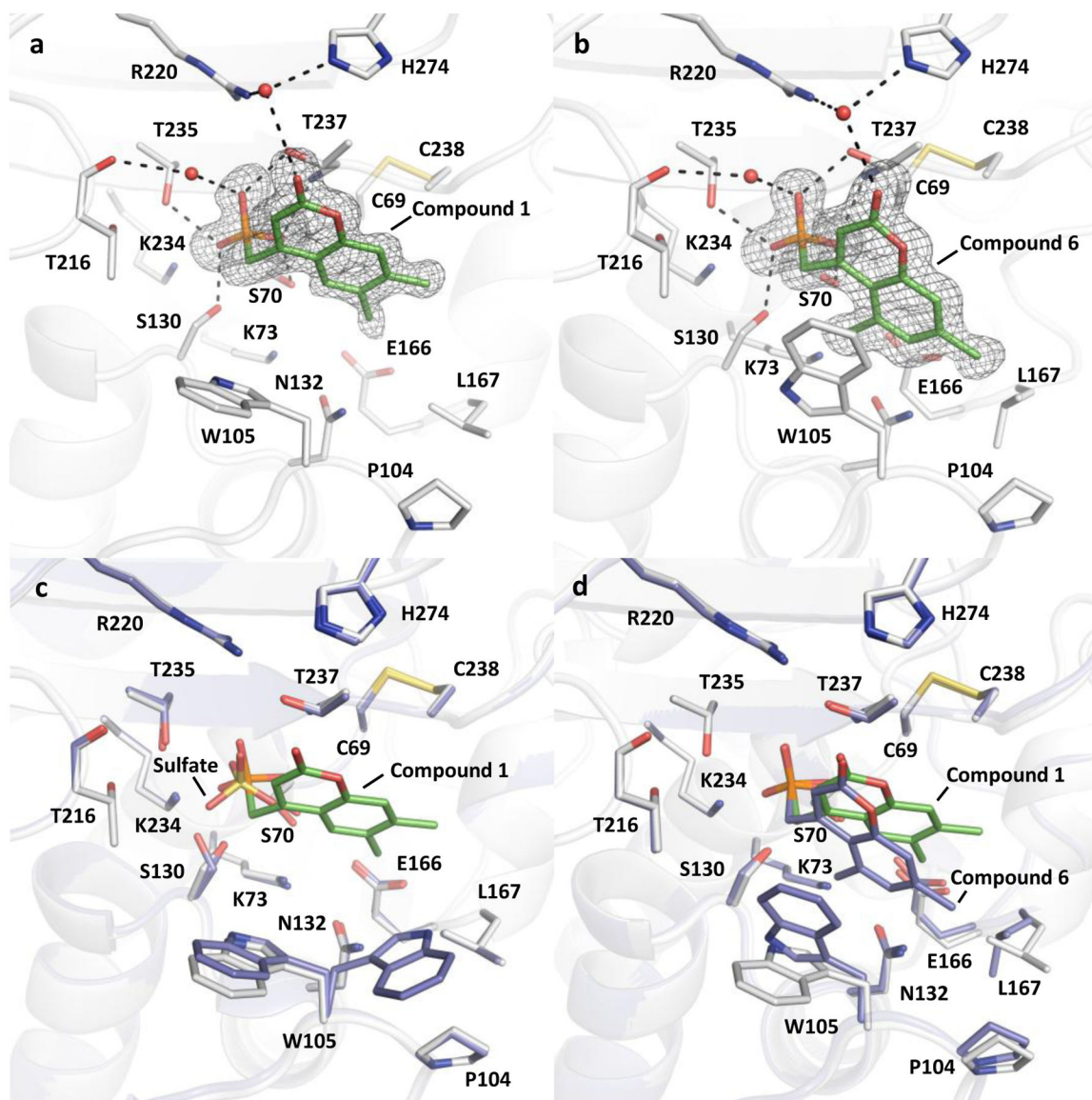


Figure 1. Crystal structures reveal binding mode of coumarin phosphonate analogs 1 and 6 to KPC-2.

The composite simulated annealing $mF_o - DF_c$ omit maps are colored in gray and contoured at 3σ . Water molecules are shown as red spheres. Black dashed lines represent hydrogen bonds. (a) Compound 1 bound to KPC-2 (PDB ID 6D15). (b) Compound 6 bound to KPC-2 (PDB ID 6D18). (c) Compound 1 complex (white and green) superimposed onto KPC-2 apo structure (purple, PDB ID 5UL8). (d) Compound 1 complex (white and green) superimposed onto compound 2 complex (purple).

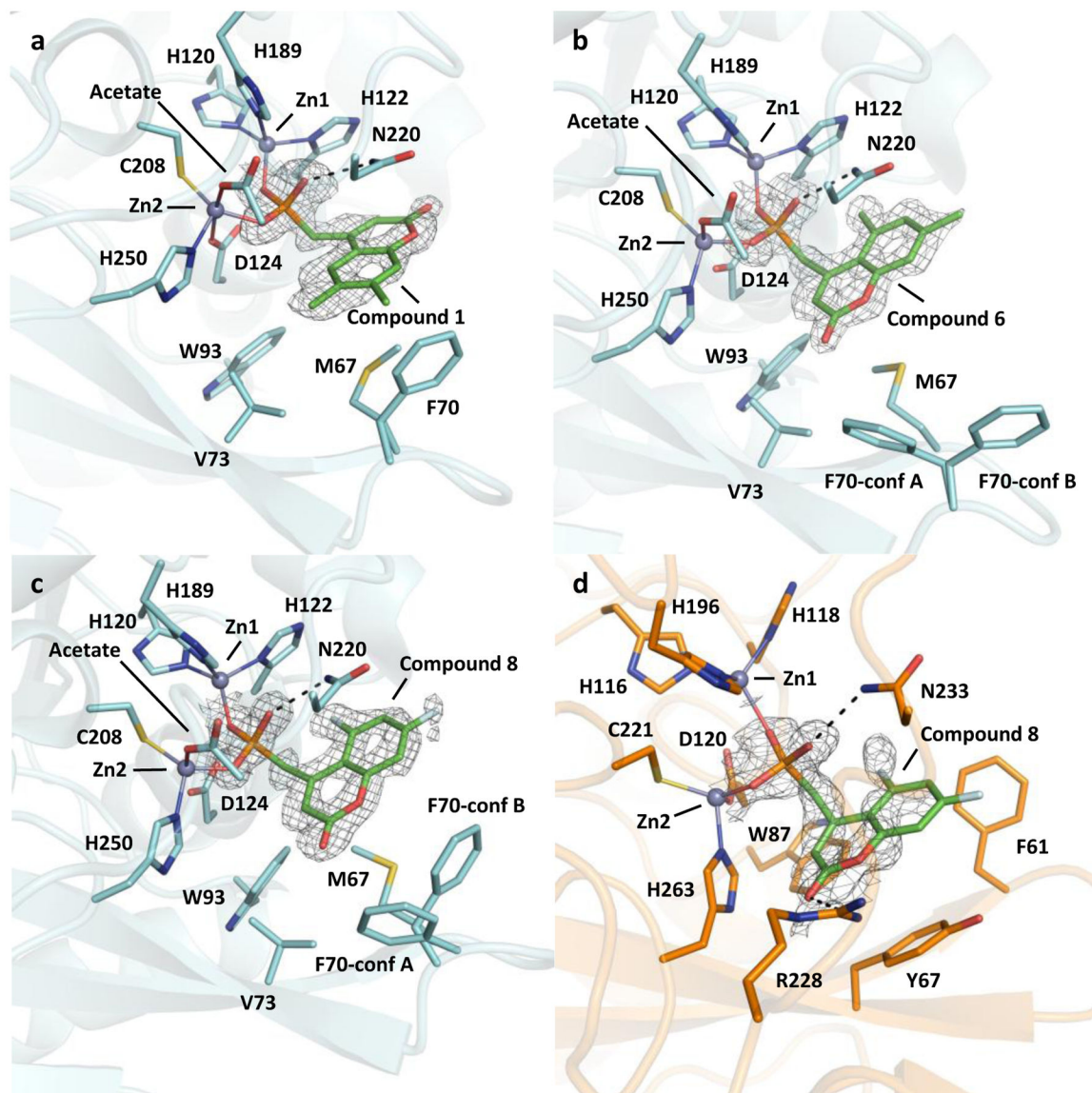


Figure 2. X-ray crystal structures of NDM-1 and VIM-2 bound to coumarin phosphonate derivatives.

The composite simulated annealing mF_o-DF_c omit maps, determined at 1.15–1.50 Å resolutions, are colored in gray and contoured at 3σ , except panel d, which has been contoured at 2σ . Black dashed lines represent hydrogen bonds. Zinc coordination is shown as thin sticks. (a) NDM-1 with **1** (PDB ID 6D1A). (b) NDM-1 with **6** (PDB ID 6D1D). (c) NDM-1 with **8** (PDB ID 6D1F). (d) VIM-2 with **8** (PDB ID 6DD0). F70 of NDM-1 adopts two conformations (labeled F70-conf A and F70-conf B) in the complex structures of **6** and **8**.

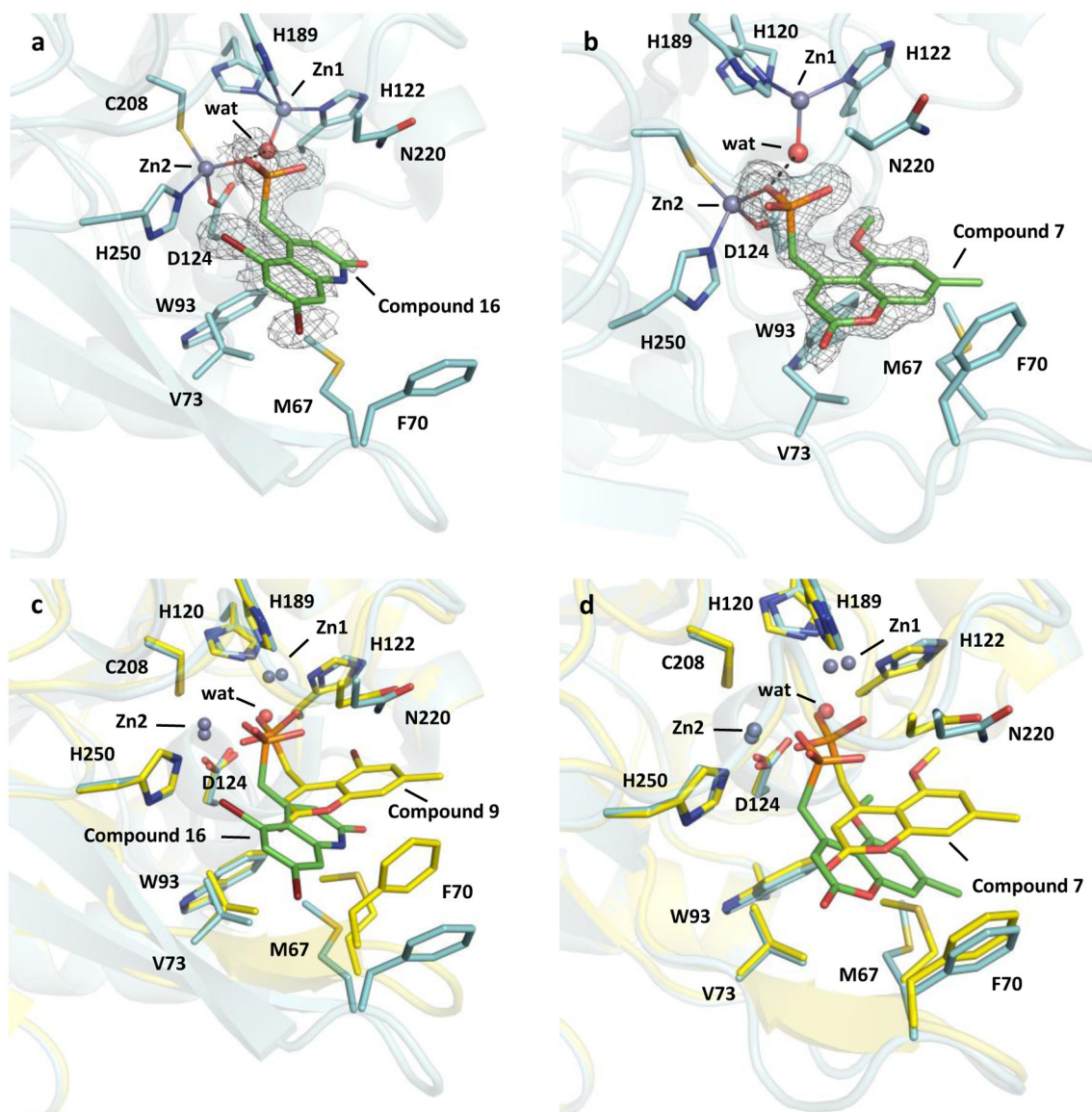


Figure 3. X-ray crystal structures of NDM-1 bound to phosphonate derivatives at pH 7.5. The composite simulated annealing mF_o-DF_c omit maps, determined at 1.30–1.40 Å resolutions, are colored in gray and contoured at 3σ . Black dashed lines represent hydrogen bonds. Zinc coordination is shown as thin sticks. (a) NDM-1 with **16** (PDB ID 6NY7). (b) NDM-1 with **7** (PDB ID 6D1E). (c) NDM-1 with **16** (light blue and green), superimposed with the NDM-1 with **9** determined at pH 3.8 (yellow, PDB ID 6D1G). (d) NDM-1 with **7** (light blue and green), superimposed with the same complex determined at pH 3.8 (yellow, PDB ID 6D1E).

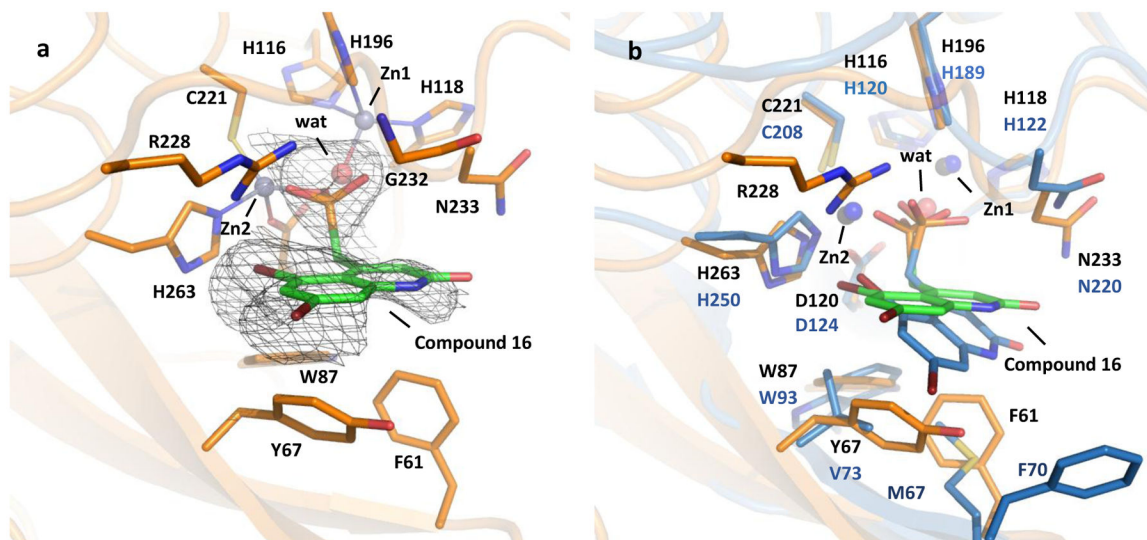


Figure 4. X-ray crystal structures of VIM-2 bound to phosphonate derivative 16 at pH 7.5. The composite simulated annealing mF_o-DF_c omit map, determined at 2.1 Å resolution, is colored in gray and contoured at 2σ . Black dashed lines represent hydrogen bonds. Zinc coordination is shown as thin sticks. (a) VIM-2 with **16** (PDB ID 6O5T). (b) VIM-2 with **16** (orange and green) superimposed with the complex of NDM-1 and **16** (blue, PDB ID 6NY7).

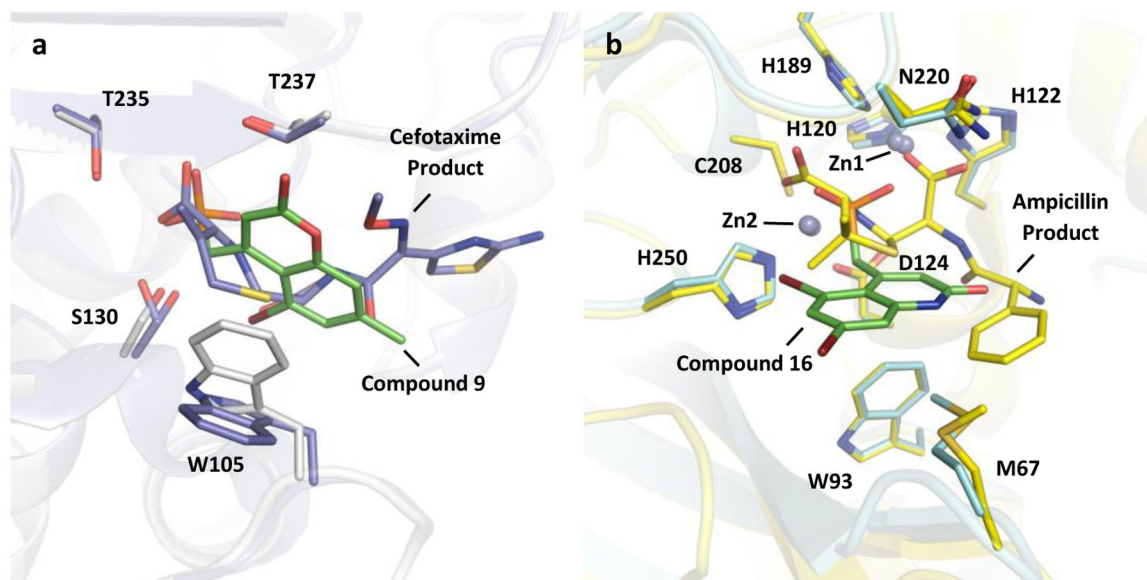
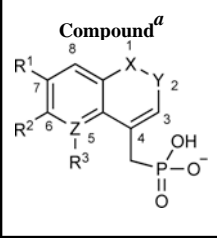


Figure 5. Superimposition of carbapenemase inhibitor and product complexes.

(a) Superimposition of KPC-2/compound **9** (white and green, PDB ID 6D19) and KPC-2/cefotaxime product (purple, PDB ID 5UJ3). (b) Superimposition of NDM-1/compound **16** (light blue and green, PDB ID 6NY7) and NDM-1/ampicillin product (yellow, PDB ID 4HL2).

Table 1.

Biochemical activities of phosphonate compounds against KPC-2, NDM-1 and VIM-2.

 Compound ^a	X	Y	Z	R ¹	R ²	R ³	K _i (KPC-2) μM	L.E. ^a (KPC-2)	K _i (NDM-1) μM	K _i (VIM-2) μM
1	O	C=O	C	Me	Me	H	32.9 ± 3.3	0.34	44.3 ± 7.3	2.1 ± 0.1
2	O	C=O	C	OMe	H	H	8.4 ± 0.4	0.39	123.7 ± 3.6	2.1 ± 0.2
3	O	C=O	C	OCH ₂ O		H	15.3 ± 2.5	0.35	N/A ^b	N/A
4	O	C=O	C	Me	H	H	23.3 ± 4.6	0.38	N/A	N/A
5 ^c	O	C=O	C	H	Me	H	154.4	0.31	N/A	N/A
6	O	C=O	C	Me	H	Me	1.4 ± 0.2	0.45	33.8 ± 3.8	0.82 ± 0.1
7	O	C=O	C	Me	H	OMe	11.9 ± 1.1	0.36	N/A	N/A
8	O	C=O	C	F	H	F	9.3 ± 1.8	0.39	No inhib	3.3 ± 0.1
9	O	C=O	C	Me	H	Br	0.246 ± 0.047	0.49	34.2 ± 8.0	1.20 ± 0.16
10	O	C=O	C	Me	H	F	8.5 ± 0.3	0.39	230.2 ± 3.2	3.3 ± 0.03
11	NH	C=O	C	H	H	H	142.3 ± 22.3	0.33	190.2 ± 22.6	6.4 ± 0.04
12	NMe	C=O	C	H	H	H	101.5 ± 8.6	0.32	81.0 ± 12.8	7.5 ± 0.02
13	NH	C=O	C	Me	H	Me	2.2 ± 0.8	0.43	56.2 ± 4.3	3.4 ± 0.03
14	C=C		N	H	H	-	730.4 ± 87.4	0.27	741.3 ± 53.1	22.3 ± 1.3
15	N=C		C	H	H	H	326.1 ± 56.8	0.30	No inhib	30.3 ± 3.2
16	NH	C=O	C	Br	H	Br	0.020 ± 0.007	0.59	31.4 ± 1.9	0.316 ± 0.015

^aL.E. = Ligand Efficiency in units of kcal mol⁻¹ number of heavy atom⁻¹ or kcal mol⁻¹ HA⁻¹^bN/A, not tested.^cCompound 5 was tested only once due to limited availability.

Table 2.

In vitro activity (MIC) of imipenem against bacterial strains expressing KPC-2, NDM-1, and VIM-2 in the presence of 9, 11, 13.

Bacterial strain	Characterized β -lactamase	Imipenem ($\mu\text{g/mL}$)	Imipenem/Compound 9 ($\mu\text{g/mL}$)	Imipenem/Compound 11 ($\mu\text{g/mL}$)	Imipenem/Compound 13 ($\mu\text{g/mL}$)	Ceftazidime/Avibactam ($\mu\text{g/mL}$)
<i>E. coli</i> 5980	NDM-1	8	2	2	2	>64/4
<i>K. pneumoniae</i> 4683	KPC-2	64	1	4	1	1/4
<i>K. pneumoniae</i> 5979	NDM-1	>64	32	32	64	>64/4
<i>E. cloacae</i> 5981	NDM-1	2	2	2	2	2/4
<i>P. aeruginosa</i> 4698	VIM-2	>64	>64	>64	>64	32/4

^aCompound 9, 11, and 13 were tested at a concentration of 128 $\mu\text{g/mL}$.

^bCeftazidime and 4 $\mu\text{g/mL}$ avibactam was included as a positive control.

Table 3.

In vitro activity (MIC) of imipenem against bacterial strains expressing KPC-2, NDM-1, and VIM-2 in the presence of 16

Bacterial strain	Characterized β -lactamase	Imipenem ($\mu\text{g/mL}$)	Imipenem+16 ($\mu\text{g/mL}$)	
			imipenem	16
<i>K. pneumoniae</i> C2	KPC-2	512	16	16
			4	128
<i>P. aeruginosa</i> 4135	KPC-2	64	2	128
<i>P. aeruginosa</i> 4129	NDM-1	128	8	128
<i>P. aeruginosa(eflx+)</i> 4177	NDM-1	128	32	128
<i>P. aeruginosa</i> 4882	VIM-2	32	2	128
<i>P. aeruginosa(eflx+)</i> 4402	VIM-2	32	4	128
<i>P. aeruginosa</i> 4173	vector	2	-	-
<i>P. aeruginosa(eflx+)</i> 4175	vector	2	-	-

^aThe *P. aeruginosa* strains (without *eflx+*) lack major efflux pumps MexAB-OprM and MexXY-OprM. The *eflx+* strain overexpresses MexAB-OprM.

Table 4.*In vitro* ADME data for compound 16 and controls.

liver microsome stability (mouse)		
compound	t _{1/2} (min)	CL _{int} (μL/min/mg protein)
verapamil	8.6 ± 0.1	161.9 ± 2.7
16	>120	< 11.6
kinetic solubility in pH 7.4 PBS		
compound	μM	μg/mL
13	193	51.6
16	241	95.9

MDCK-MDR cell permeability			
compound	Papp _{A-B} (x10 ⁻⁶ cm/s)	Papp _{B-A} (x10 ⁻⁶ cm/s)	recovery (%)
digoxin	0.4	16.5	105
propranolol	57.5	34.9	97
16	< 0.7	< 0.2	91